JHEP

Published for SISSA by Springer

Received: *September 10, 2021*
Revised: *December 5, 2021*
Accepted: *December 24, 2021*
Published: *January 14, 2022*

ZZ production at nNNLO+PS with MiNNLO$_{\mathrm{PS}}$

Luca Buonocore,[a] **Gabriël Koole,**[b] **Daniele Lombardi,**[b] **Luca Rottoli,**[a] **Marius Wiesemann**[b] **and Giulia Zanderighi**[b]

[a] *University of Zurich, Winterthurerstrasse 190, 8057 Zurich, Switzerland*
[b] *Max-Planck-Institut für Physik, Föhringer Ring 6, 80805 München, Germany*

E-mail: lbuono@physik.uzh.ch, koole@mpp.mpg.de, lombardi@mpp.mpg.de, lrotto@physik.uzh.ch, wieseman@mpp.mpg.de, zanderi@mpp.mpg.de

Abstract: We consider ZZ production in hadronic collisions and present state-of-the-art predictions in QCD perturbation theory matched to parton showers. Next-to-next-to-leading order corrections to the quark-initiated channel are combined with parton showers using the MiNNLO$_{\mathrm{PS}}$ method, while next-to-leading order corrections to the loop-induced gluon fusion channel are matched using the Powheg method. Their combination, dubbed nNNLO+PS, constitutes the best theoretical description of ZZ events to date. Spin correlations, interferences and off-shell effects are included by calculating the full process $pp \to \ell^+\ell^-\ell^{(\prime)+}\ell^{(\prime)-}$. We show the crucial impact of higher-order corrections for both quark- and gluon-initiated processes as well as the relevance of the parton shower in certain kinematical regimes. Our predictions are in very good agreement with recent LHC data.

Keywords: QCD Phenomenology

ArXiv ePrint: 2108.05337

https://doi.org/10.1007/JHEP01(2022)072

JHEP01(2022)072

Contents

1 Introduction

Vector-boson pair production processes provide some of the most relevant signatures in precision measurements, which have evolved to one of the cornerstones of the rich physics programme at the Large Hadron Collider (LHC). The accurate determination of production rates and distributions provides a valuable path towards the observation of deviations from the predictions made by the Standard Model (SM) of particle physics. Observing or constraining anomalous interactions among SM particles is one of the central goals of such analyses. Through diboson signatures the couplings among three vector bosons (triple-gauge couplings) are directly accessible, which are altered by various beyond-the-SM (BSM) theories. Therefore, the observation of small deviations from the expected rates or shapes of distributions would be a clear sign of new physics. Similarly, measurements at high transverse momentum of some of the particles produced in diboson processes provide constraints on the mass range of possible heavy Z' bosons. Apart from that, vector-boson pair final states constitute an irreducible background to on- and off-shell Higgs cross-section measurements, when the Higgs boson decays to four leptons. These measurements are important for the extraction of the Higgs couplings and for constraints of the Higgs width [1–11].

While the cross section for ZZ production is smaller than the one of $W^{\pm}Z$ or $W^{+}W^{-}$ production, experimentally the decay to four charged leptons provides the cleanest signature of the massive diboson processes, since the final state does not involve any missing

JHEP01(2022)072

transverse momentum. Accordingly, experimental measurements already reach a remarkable level of precision. In particular, both ATLAS and CMS collaborations have performed measurements of the ZZ production cross sections at 5.02 TeV [12], 7 TeV [13–16], 8 TeV [16–21] and 13 TeV [21–26] and used these measurements to test the SM and constrain triple-gauge couplings.

Modern fits of parton distribution functions (PDFs) have started to include more and more LHC data. For instance NNPDF3.1 [27] already includes top-pair production and the transverse momentum of the Drell-Yan pair. Upcoming fits will also include direct photon, dijet and single top production. It is clear that a further step would be the inclusion of diboson production and other processes with more final-state particles such as three jets, provided the accuracy of theory predictions, both at the level of higher-order QCD and electroweak (EW) corrections, is sufficient.

The first next-to-leading order (NLO) QCD corrections to Z-boson pair production started to appear about thirty years ago [28–32]. NLO QCD calculations were later consistently matched with fully exclusive Parton Shower Monte Carlo programmes (NLO+PS) using the POWHEG [33, 34] or aMC@NLO method [35]. Electroweak (EW) effects at NLO were also computed first in the on-shell approximation [36, 37] and later keeping off-shell and spin-correlation effects [38, 39]. The combination of NLO QCD and NLO EW corrections was presented in ref. [40] and recently also their matching to parton showers was performed [41]. Likewise, in the case of polarized Z bosons NLO QCD and NLO EW corrections have been combined very recently [42]. NNLO QCD corrections have been computed for on-shell [43, 44] and off-shell ZZ production [45, 46], and their combination with NLO EW effects was presented in ref. [47]. The loop-induced $gg \to ZZ$ process starts contributing only at $\mathcal{O}(\alpha_s^2)$, but it is enhanced by the gluon PDFs. Since higher-order corrections to this process can be formulated as a gauge-invariant set of contributions and their impact was expected to be important, NLO QCD corrections to $gg \to ZZ$ production have also been computed in the recent years [5, 48–50]. The leading order (LO) matching of the loop-induced gluon fusion process was presented in ref. [51], while NLO+PS predictions were first obtained neglecting the quark channels [52] and very recently also including the full NLO QCD corrections with quark-gluon and quark-antiquark channels and the Higgs resonance [53].

The remarkable progress in NNLO QCD calculations[1] triggered considerable advancements in the matching of NNLO QCD corrections and parton showers (NNLO+PS). The first method developed was the NNLOPS method based on MINLO′ [89, 90], which achieves NNLO QCD accuracy through a reweighting of MINLO′ events. This method was successfully employed for relatively simple processes, such as Higgs production [90], Drell-Yan production [91] and associated Higgs production [92, 93], i.e. to processes that from a QCD point of view are just $2 \to 1$ processes. The same method was then also employed for W^+W^- production, including the decay of the W-bosons [94]. This paper showed explicitly the limitations of the NNLOPS method, because in practice the multi-differential reweighting can not easily be applied to more complicated processes, without making cer-

[1] By now all $2 \to 1$ and $2 \to 2$ colour-singlet processes are available at NNLO QCD [43–46, 54–83] (see e.g. ref. [84] for a review), and even first such calculations for $2 \to 3$ processes are emerging [85–88].

JHEP01(2022)072

tain assumptions or approximations. About ten years ago, two more NNLO+PS methods were proposed: the UNNLOPS one, which has only been applied to Higgs [95] and Drell-Yan production [96], and the GENEVA method [97, 98]. The latter was subsequently modified, as far as the interface to the shower is concerned, and applied to Drell-Yan [99], Higgsstrahlung [100], photon pair production [101], hadronic Higgs decays [102], ZZ production [103], and $W\gamma$ production [104]. Recently, the GENEVA method was reformulated using the transverse momentum of the colour singlet rather than the jettiness variable and applied to Drell-Yan [105].

Two years ago, the MINNLO$_{\text{PS}}$ method was proposed [106, 107], whose underlying idea is very similar to the MINLO$'$ approach that achieves NLO accuracy for colour singlet plus zero and one jet simultaneously. The MINNLO$_{\text{PS}}$ method exploits the close connection to transverse-momentum resummation to include the relevant logarithmically enhanced and constant terms to reach NNLO accuracy. This method was first used to reproduce known results for Higgs production and Drell-Yan [106, 107] and it was applied more recently to $Z\gamma$ [108] and W^+W^- production [109]. Remarkably, although it was the last NNLO+PS method to appear, the MINNLO$_{\text{PS}}$ method was the first to be extended and applied to the production of a coloured final state, namely top-quark pair production [110].

In this work, we employ the MINNLO$_{\text{PS}}$ method to include NNLO QCD corrections for ZZ production in the POWHEG framework. Additionally, we present a NLO+PS POWHEG calculation for the loop-induced $gg \to ZZ$ process. When combined, these predictions, dubbed nNNLO+PS, become the most advanced theoretical predictions for ZZ production at the LHC, since they include the highest perturbative accuracy in QCD available to date. Spin correlations, interferences and off-shell effects are included by considering all contributions to the four-lepton final state. Moreover, the matching to the parton shower renders it possible to achieve a fully exclusive description at the level of hadronic events. In the future, the NNLO+PS predictions of our MINNLO$_{\text{PS}}$ ZZ generator could be compared to those recently obtained in the GENEVA framework [103].

This manuscript is organized as follows: in section 2 we discuss in detail the calculation and implementation of the MINNLO$_{\text{PS}}$ method for the $q\bar{q}$-initiated process and the POWHEG implementation for the loop-induced gg-initiated process. We also show how to avoid that the two-loop amplitudes, whose numerical evaluation is very time-consuming, slow down our code in a considerable way. Our phenomenological results for both cross sections and distributions in ZZ production are discussed in section 3, where we present a comparison between showered, fixed-order, and analytically resummed results at high accuracy for various observables as well as a comparison of our nNNLO+PS predictions to recent LHC data from CMS. We conclude in section 4.

2 Outline of the calculation

2.1 Description of the process

We study the process

$$pp \to \ell^+\ell^-\ell^{(\prime)+}\ell^{(\prime)-} \tag{2.1}$$

for any combination of charged leptons $\ell, \ell' \in \{e, \mu, \tau\}$. While at the matrix-element level our calculation is based on the different-flavour channel $\ell \neq \ell'$, at the event-generation level

JHEP01(2022)072

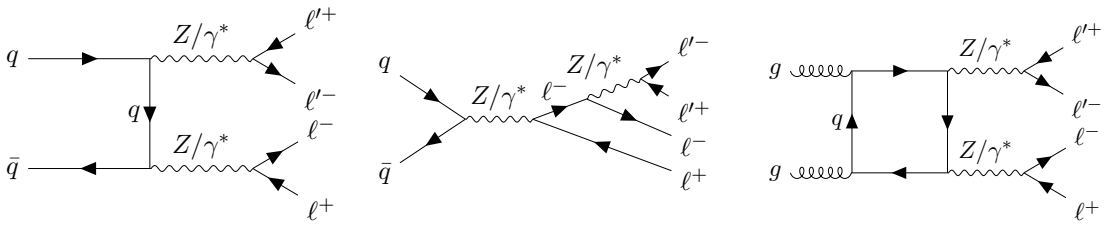

Figure 1. Sample Feynman diagrams for ZZ production with four charged leptons in the final state. Panels (a) and (b): tree-level diagrams of the quark annihilation ($q\bar{q}$) channel; Panel (c): loop-induced diagram in the gluon fusion (gg) channel.

arbitrary combinations of charged leptons can be considered, both with different flavours $\ell \neq \ell'$ and with same flavours $\ell = \ell'$ (in the latter case interference effects when exchanging the charged leptons, which are typically at the 1-2% level [45], are neglected). Moreover, lepton masses are included via reshuffling of the momenta in the event generation. For simplicity and without loss of generality we consider only the process $pp \to e^+e^-\mu^+\mu^-$ here, which we will refer to as ZZ production in the following. By including all resonant and non-resonant topologies leading to this process, off-shell effects, interferences and spin correlations are taken into account. Sample diagrams are shown in figure 1 and they include:

(a) tree-level double-resonant t-channel ZZ production in the $q\bar{q}$ channel;

(b) tree-level single-resonant s-channel Drell-Yan topologies in the $q\bar{q}$ channel;

(c) loop-induced ZZ production in the gg channel.

The loop-induced gg contribution, including also the single-resonant Higgs mediated diagrams, proceeds through a quark loop and enters the cross section at $\mathcal{O}(\alpha_s^2)$, i.e. it is part of the NNLO QCD corrections. Since this contribution is enhanced by the large gluon-gluon luminosity at LHC energies, it yields a relatively large fraction of the NNLO corrections [73, 74]. Moreover, it is known that at NLO QCD [48, 50], i.e. $\mathcal{O}(\alpha_s^3)$, its relative correction is very sizable (about a factor of two). It is likely that these corrections constitute the most significant contribution to ZZ production at $\mathcal{O}(\alpha_s^3)$, since the $\mathcal{O}(\alpha_s^3)$ corrections to the $q\bar{q}$ channel are not expected to be of the same size as those at the previous order.

We include the most accurate currently available information in QCD perturbation theory for both the $q\bar{q}$-initiated and the loop-induced gg-initiated process, and match them consistently with a parton shower. Thus, we calculate NNLO+PS predictions in the $q\bar{q}$ channel by means of the MiNNLO$_{\text{PS}}$ method [106–108] and NLO+PS predictions in the loop-induced gg channel using the Powheg approach [111–113]. Full top-quark mass effects are included everywhere, except for the two-loop amplitudes. For the $q\bar{q}$ channel they are expected to be small in the relevant phase-space regions, while for the loop-induced gg contribution we have included them approximately via reweighting in the two-loop correction (cf. section 2.3). We stress that to avoid any overlap, our MiNNLO$_{\text{PS}}$ implemen-

JHEP01(2022)072

tation of the NNLO+PS calculation in the $q\bar{q}$ channel does not include the loop-induced gg-initiated contribution. In this way, all loop-induced gg contributions are correctly accounted for when combining the former with our NLO+PS predictions for the gg channel. Our ensuing result is dubbed as nNNLO+PS, as the NLO corrections to the loop-induced gluon-fusion contribution are of $\mathcal{O}(\alpha_s^3)$. These corrections are separately gauge-invariant and constitute the most significant N^{3}LO corrections, as pointed out before.

2.2 MiNNLO$_{\text{PS}}$ for $q\bar{q} \to ZZ$ production

In this section we present the implementation of a NNLO+PS generator for ZZ production in the $q\bar{q}$ channel by means of the MiNNLO$_{\text{PS}}$ method. We first sketch the MiNNLO$_{\text{PS}}$ method by introducing its essential ingredients and then discuss its practical implementation within the Powheg-Box-Res framework [114] and linking Matrix [115].

2.2.1 The MiNNLO$_{\text{PS}}$ method for colour-singlet production

MiNNLO$_{\text{PS}}$ has been formulated in ref. [106], optimized for $2 \to 1$ processes in ref. [107] and later extended to generic colour-singlet processes in ref. [108] and to heavy-quark pair production in ref. [110]. We refer to those publications for a detailed description of the MiNNLO$_{\text{PS}}$ method and here we only sketch the procedure adopting a simplified notation.

The MiNNLO$_{\text{PS}}$ method includes NNLO corrections in the event generation of a system F of colour-singlet particles. It involves essentially three steps: in the first one (Step I) F is generated in association with one light parton at NLO according to the Powheg method [111–113, 116], inclusively over the radiation of a second light parton. The second step (Step II) characterizes the MiNNLO$_{\text{PS}}$ approach, and it corrects the limit in which the light partons become unresolved by supplementing the appropriate Sudakov form factor and higher-order terms, such that the simulation remains finite as well as NNLO accurate for inclusive F production. In the third step (Step III), the kinematics of the second radiated parton (accounted for inclusively in Step I) is generated through the Powheg method to preserve the NLO accuracy of the F+1-jet cross section, and subsequent radiation is included through the parton shower. In these three steps all emissions are appropriately ordered (when using a p_{T}-ordered shower) and the applied Sudakov matches the leading logarithms resummed by the parton shower. Thus, the MiNNLO$_{\text{PS}}$ approach preserves the (leading logarithmic) accuracy of the parton shower.

The fully differential MiNNLO$_{\text{PS}}$ cross section can be expressed through the Powheg formula for the production of a colour singlet plus one light parton (FJ) with a modified content of the $\bar{B}$ function:

$$\mathrm{d}\sigma_{\text{F}}^{\text{MiNNLO}_{\text{PS}}} = \mathrm{d}\Phi_{\text{FJ}}\, \bar{B}^{\,\text{MiNNLO}_{\text{PS}}} \times \left\{ \Delta_{\text{pwg}}(\Lambda_{\text{pwg}}) + \mathrm{d}\Phi_{\text{rad}} \Delta_{\text{pwg}}(p_{\text{T,rad}}) \frac{R_{\text{FJ}}}{B_{\text{FJ}}} \right\}, \tag{2.2}$$

where Δ_{pwg} is the Powheg Sudakov form factor, Φ_{FJ} is the phase space of the FJ system, Φ_{rad} and $p_{\text{T,rad}}$ are the phase space and the transverse momentum of the second radiation, respectively, and B_{FJ} and R_{FJ} denote the squared tree-level matrix elements for FJ and FJJ production, respectively. The content of the curly brackets generates the second QCD emission according to the Powheg method, as described in Step III above, with a default

JHEP01(2022)072

cutoff of $\Lambda^2_{\rm pwg} = 0.8\,{\rm GeV}^2$. The $\bar{B}$ function contains the same contributions to generate the first emission (and inclusively the second emission) as in a standard FJ POWHEG calculation, described in Step I above, but it is modified according to the MINNLO$_{\rm PS}$ procedure in order to reach NNLO accuracy for inclusive F production, as discussed in Step II above. Symbolically, it can be written as

$$\bar{B}^{\,\rm MiNNLO_{PS}} \sim e^{-S}\left\{{\rm d}\sigma^{(1)}_{\rm FJ}(1+S^{(1)}) + {\rm d}\sigma^{(2)}_{\rm FJ} + \left(D - D^{(1)} - D^{(2)}\right)\times F^{\rm corr}\right\}, \tag{2.3}$$

with ${\rm d}\sigma^{(1,2)}_{\rm FJ}$ being the first- and second-order contribution to the differential FJ cross section and e^{-S} denoting the Sudakov form factor for the transverse momentum of F. Note that in the MINNLO$_{\rm PS}$ approach the renormalization and factorization scales are evaluated as $\mu_{\rm R} \sim \mu_{\rm F} \sim p_{\rm T}$, where $p_{\rm T}$ is the transverse momentum of F. The third term in eq. (2.3) is of order $\alpha_s^3(p_{\rm T})$ and it adds the relevant (singular) contributions so that the integration over $p_{\rm T}$ yields a NNLO accurate result [106]. Regular contributions at this order are of subleading nature. The function D is derived from the transverse-momentum resummation formula, which can be expressed fully differentially in the Born phase space of F as

$${\rm d}\sigma^{\rm res}_{\rm F} = \frac{\rm d}{{\rm d}p_{\rm T}}\left\{e^{-S}\mathcal{L}\right\} = e^{-S}\underbrace{\left\{-S'\mathcal{L}+\mathcal{L}'\right\}}_{\equiv D}, \tag{2.4}$$

with $\mathcal{L}$ being the luminosity factor up to NNLO that includes the squared hard-virtual matrix elements for F production and the convolution of the collinear coefficient functions with the parton distribution functions (PDFs). In fact, eq. (2.3) follows directly from matching eq. (2.4) with the fixed-order cross section ${\rm d}\sigma_{\rm FJ}$, when using a matching scheme where the Sudakov form factor is factored out, i.e.

$$\begin{aligned}
&{\rm d}\sigma^{\rm res}_{\rm F} + [{\rm d}\sigma_{\rm FJ}]_{\rm f.o.} - [{\rm d}\sigma^{\rm res}_{\rm F}]_{\rm f.o.} \\
&\quad = e^{-S}\left\{D + [{\rm d}\sigma_{\rm FJ}]_{\rm f.o.}\underbrace{\frac{1}{[e^{-S}]_{\rm f.o.}}}_{1+S^{(1)}\ldots} \underbrace{- \frac{[{\rm d}\sigma^{\rm res}_{\rm F}]_{\rm f.o.}}{[e^{-S}]_{\rm f.o.}}}_{-D^{(1)}-D^{(2)}\ldots}\right\} \\
&\quad = e^{-S}\left\{{\rm d}\sigma^{(1)}_{\rm FJ}(1+S^{(1)}) + {\rm d}\sigma^{(2)}_{\rm FJ} + \left(D - D^{(1)} - D^{(2)}\right) + \mathcal{O}(\alpha_s^4)\right\},
\end{aligned} \tag{2.5}$$

where $[\cdots]_{\rm f.o.}$ denotes the expansion up to a given fixed order in α_s. Finally, $F^{\rm corr}$ in eq. (2.3) determines the appropriate function to spread the NNLO corrections in the FJ phase space, which is necessary to include those corrections in the context of an FJ POWHEG calculation. Note also that one could either truncate the third term in eq. (2.3) at the third order $\left(D - D^{(1)} - D^{(2)}\right) = D^{(3)} + \mathcal{O}(\alpha_s^4)$ [106], or keep the terms of $\mathcal{O}(\alpha_s^4)$ and higher [107], which are beyond accuracy, in order to preserve the total derivative in eq. (2.4). We employ the latter option here.

2.2.2 Practical implementation in POWHEG-BOX-RES+MATRIX

In the following we provide some information on our implementation of a MINNLO$_{\rm PS}$ generator for ZZ production in the $q\bar{q}$ channel within the POWHEG-BOX-RES framework [114].

JHEP01(2022)072

Our NLO+PS generator for the loop-induced gg channel is discussed in the next section. We stress that, while we distinguish these processes as $q\bar{q}$ and gg, in their higher-order corrections of course all the relevant partonic initial states are consistently included, with the exception of the gg loop-induced partonic channel in the NNLO corrections to the $q\bar{q}$ process, since this contribution is already accounted for by our NLO+PS generator for the loop-induced gg channel.

Since no implementation for ZZ+jet production was available in POWHEG-BOX to date, the first step was to implement this process in the POWHEG-BOX-RES framework. We have implemented all relevant flavour channels and, in addition, adapted the routine `build_resonance_histories` of POWHEG-BOX-RES such that it is capable of automatically constructing the correct resonance histories. The tree-level single and double real matrix elements for $e^+e^-\mu^+\mu^-$+1, 2-jet production and the one-loop amplitude for $e^+e^-\mu^+\mu^-$+1-jet production are evaluated through OPENLOOPS [117–119].

In a second step, we have employed the MINNLO$_{\text{PS}}$ method to obtain NNLO+PS predictions for ZZ production in the $q\bar{q}$ channel. In particular, we made use of the implementation of the MINNLO$_{\text{PS}}$ method that was developed and applied to $Z\gamma$ production in ref. [108]. The respective tree-level and one-loop $q\bar{q} \to e^+e^-\mu^+\mu^-$ amplitudes are also evaluated through OPENLOOPS, while the two-loop helicity amplitudes have been obtained by extending the interface to MATRIX [115] developed in ref. [108] to ZZ production. The evaluation of the two-loop coefficients in this implementation relies on the code VVAMP [120] and is based on the calculation of ref. [121].

As discussed in ref. [109] for W^+W^- production, the evaluation of the two-loop helicity amplitudes for massive diboson processes is particularly demanding from a computational point of view. In ref. [109] this problem was circumvented by constructing a set of interpolation grids for the two-loop coefficients that achieves their fast on-the-fly evaluation. In this work we pursue a different strategy: we exploit the possibility of reweighting the events at the generation level (i.e. stage 4 in POWHEG-BOX) to include the two-loop contribution. In combination with a suitable caching system of the two-loop amplitude that we implemented this allows us to omit the evaluation of the two-loop contribution entirely in the calculation up to stage 4, where it needs to be evaluated only once per event.[2] To be more precise, we have implemented a new flag (`run_mode`), which is accessible from the POWHEG input file, and allows the user to switch between four different ways of running the code. Either the full calculation is performed including the two-loop contributions throughout (`run_mode 1`), or one completely drops the NNLO corrections provided by MINNLO$_{\text{PS}}$, specifically the terms $\left(D - D^{(1)} - D^{(2)}\right) \times F^{\text{corr}}$ in eq. (2.3), thus effectively reproducing MINLO′ predictions (`run_mode 2`). Alternatively, the evaluation of two-loop amplitude can be omitted only in the grid setup, i.e. stage 1 in POWHEG-BOX, (`run_mode 3`), or completely (`run_mode 4`). For all results presented in this manuscript we run the code with the last option `run_mode 4`, i.e. without evaluating the computationally expensive two-loop amplitude. In this way, also the generation of the events is faster. However, once an event has

[2]Note that in order for the caching to work properly and not having to reevaluate the two-loop amplitude for every scale variation in the event reweighting, we have set the parameter `rwl_group_events 1` in the input file, which ensures that the events are reweighted one-by-one instead of in batches.

JHEP01(2022)072

been accepted, it is reweighted such that the two-loop contribution is included by resetting the `run_mode` keyword in the event reweight information of the POWHEG input file. As a result the two-loop amplitude is evaluated only once for each event, considerably improving the efficiency of the code. Moreover, following the same logic we can also compute MINLO′ weights in parallel to the generation of MINNLO$_{\rm PS}$ ones using the appropriate setting for `run_mode` in the event reweight information. We have first validated our implementation in an inclusive setup, requiring only a suitable Z-mass window for the opposite-charge same-flavour dilepton pairs. Here we compared the inclusive cross section at the Les Houches event (LHE) level obtained at stage 4 with the one computed at stage 2 when including the two-loop contribution, finding excellent agreement. Another very robust cross-check of the reweighting procedure is provided by the comparison of the MINLO′ results obtained directly or through reweighting, which also agree perfectly.

Our calculation involves the evaluation of several convolutions with the PDFs, for which we employ HOPPET [122]. The evaluation of the polylogarithms entering the collinear coefficient functions is done through the HPLOG package [123].

Finally, let us summarize some of the most relevant (non-standard) settings that we have used to produce NNLO+PS accurate ZZ events in the $q\bar{q}$ channel. For more detailed information on those settings we refer to refs. [107, 110]. To avoid spurious contributions from higher-order logarithmic terms at large $p_{\rm T}$, we replace the logarithm $L = \ln Q/p_{\rm T}$, where we set $Q = m_{4\ell}$, with a modified logarithm $\tilde{L}$ which is identical to L below $p_{\rm T} = Q/2$ and smoothly vanishes at $p_{\rm T}$ equal or larger than Q [110]. As far as the renormalization and factorization scales are concerned, we use the standard MINNLO$_{\rm PS}$ scale setting at small $p_{\rm T}$ [107],

$$\mu_{\rm R} = K_{\rm R}\, Q\, e^{-\tilde{L}}\,, \qquad \mu_{\rm F} = K_{\rm F}\, Q\, e^{-\tilde{L}}\,, \tag{2.6}$$

where $K_{\rm R,F}$ are scale variation parameters varied between 1/2 and 2. In the NLO ZZ+jet cross section at large $p_{\rm T}$ the scale setting is changed to [107]

$$\mu_{\rm R} = K_{\rm R}\, p_{\rm T}\,, \qquad \mu_{\rm F} = K_{\rm F}\, p_{\rm T}\,, \tag{2.7}$$

by activating the option `largeptscales 1`. The Landau singularity is regulated by freezing the strong coupling and the PDFs for scales below 0.8 GeV. Finally, as recommended for processes with jets in the final state, we turn on the option `doublefsr 1` of the POWHEG-BOX, see ref. [124] for details. For the parton-shower we have used the standard settings, also for the recoil scheme (namely a global recoil scheme for initial state radiation, with `SpaceShower:dipoleRecoil 0`).

2.3 NLO+PS for $gg \to ZZ$ production

As discussed before, the leading-order contribution to the loop-induced gluon fusion process enters the ZZ cross section at $\mathcal{O}(\alpha_s^2)$. Thus, it constitutes a NNLO correction relative to the LO part of the $q\bar{q}$ channel, but it is significantly enhanced by the large gluon-gluon luminosities. It is therefore mandatory to include also the NLO corrections to the loop-induced gluon fusion contribution in any precision study of ZZ production that compares theory and data.

JHEP01(2022)072

We have implemented a NLO+PS generator for loop-induced ZZ production in the gg channel within the POWHEG-BOX-RES framework. Note that in addition to continuum ZZ production as shown in figure 1 (c) we also include the contribution mediated by a Higgs boson (or a single Z boson). The calculation of these loop-induced processes is effectively of similar complexity as a NNLO calculation, as far as the amplitude evaluation is concerned. Despite that, the matching to the parton shower through the POWHEG method, which is essentially automated in POWHEG-BOX-RES, can be applied to loop-induced processes as well, without any further conceptual issues. However such an NLO calculation requires the evaluation of both one-loop and two-loop helicity amplitudes and the process at hand is numerically substantially more demanding than a tree-level one, since the evaluation time of the one-loop and two-loop amplitudes is much slower and the stability of the one-loop matrix elements with one emitted real parton is challenged in the infrared regions. To cope with these numerical issues, we have implemented and exploited a number of handles within POWHEG-BOX-RES, which will be discussed below.

For the implementation in POWHEG-BOX-RES, we have specified the relevant flavour channels and hard-coded also the resonance channels of the process, as the automatic determination of the latter via the already mentioned routine `build_resonance_histories` is not available yet for loop-induced processes. At NLO, all relevant partonic channels, namely gg, gq, qg, $q\bar{q}$ and the charge-conjugated ones, are included. To unambiguously define the NLO corrections to the loop-induced gluon-fusion process for each of those initial states, we follow the approach introduced in ref. [50] and include all diagrams that involve a closed fermion loop with at least one vector boson attached. The one-loop amplitudes with zero and one jet are evaluated through OPENLOOPS [117–119]. For this purpose, we have adapted the OPENLOOPS interface in POWHEG-BOX-RES developed in ref. [125] to deal with loop-induced processes. As a cross-check, we have also interfaced RECOLA to POWHEG-BOX-RES and found full agreement for all one-loop amplitudes. For the two-loop helicity $gg \to \ell^+\ell^-\ell^{(\prime)+}\ell^{(\prime)-}$ amplitudes we exploit their implementation within MATRIX [115], which is based on the evaluation of the two-loop coefficients through VVAMP [121] from their calculation in ref. [126]. To this end, we have extended the interface of POWHEG-BOX-RES to MATRIX developed in ref. [108] to include the $gg \to \ell^+\ell^-\ell^{(\prime)+}\ell^{(\prime)-}$ two-loop amplitudes. Also here the evaluation of the two-loop coefficients through VVAMP is very slow, lasting from a few seconds to several tens of seconds. Since this leads to a severe bottleneck in the calculation and especially in the event generation, we have implemented a caching system for the two-loop corrections and we include them only through event reweighting. This is very similar in spirit to the way the two-loop hard function is included in the MINNLO$_{\text{PS}}$ generator in the $q\bar{q}$ channel, as described in the previous section. Our calculation includes the full top-quark mass effects, except for the two-loop $gg \to \ell^+\ell^-\ell^{(\prime)+}\ell^{(\prime)-}$ amplitudes, where they are not known to date.[3] Instead, we follow the same approach as ref. [50] and include them approximately through a reweighting of the massless two-loop amplitude with the ratio of the one-loop result including massive loops to

[3]For the case of on-shell $gg \to ZZ$ production the full top-quark mass dependence was recently calculated in refs. [127, 128].

JHEP01(2022)072

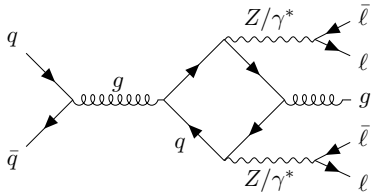

Figure 2. Sample Feynman diagram for a $q\bar{q}$-initiated regular contribution to the loop-induced gg channel at $\mathcal{O}(\alpha_s^3)$.

the one with only massless loops. Since here we are interested in the ZZ signal region, such reweighting is expected to work extremely well. In fact, ref. [53] recently confirmed that using an asymptotic expansion in the top-quark mass leads to practically identical results as using such reweighting, as long as one sticks to the validity range of the expansion itself.

Very recently, ref. [53] presented a completely independent implementation of a NLO+PS generator for loop-induced ZZ production in the gg channel within the POWHEG-BOX-RES framework. We have compared our calculation to theirs both at the level of individual phase-space points and of the integrated cross sections, and we have found perfect agreement when applying the same approximation for the two-loop virtual corrections.[4] Since, although developed independently, the two calculations are essentially interchangeable (both developed in POWHEG-BOX-RES using OPENLOOPS and VVAMP), we advocate that it is equivalent to use either code and combine the results subsequently with our MINNLOPS generator in the $q\bar{q}$ channel to obtain nNNLO+PS accurate results.

To better control the numerical stability of the calculation we have implemented settings similar to those reported in ref. [53]: in particular we apply small (0.5 GeV) generation cuts on the transverse momentum of the four-lepton system and of each Z boson. Moreover, we exploit the stability system of OPENLOOPS and set the parameter `stability_kill2 0.01` to remove the remaining unstable points. We have further modified the code in such a way that, whenever the real-emission contribution is set to zero by one of the previous stability checks, also the respective counter terms are set to zero. Finally, we use `withdamp 0` in order not to split the real cross section into a singular and a remnant contribution as the considerably small value of the latter leads to numerical issues when generating events. The same is true for the regular contribution that contains only the $q\bar{q}$ channel (see figure 2 for a sample diagram): after verifying that it is completely negligible, we have turned it off for all results obtained in this paper.

Since in the upcoming section we study phenomenological results for the full $pp \to e^+e^-\mu^+\mu^-$ process, we show some plots for the loop-induced gg channel separately in figure 3, both at LO and at NLO. The settings and inputs that we use here correspond to those introduced in section 3.1 in the inclusive setup (`setup-inclusive`) with just a Z-mass window applied between 60 GeV and 120 GeV. The renormalization and factorization scales are set to $\mu_R = \mu_F = \sqrt{m_{4\ell}^2 + p_{T,4\ell}^2}$, where $m_{4\ell}$ and $p_{T,4\ell}$ are the invariant mass and the transverse momentum of the four-lepton system, respectively. Furthermore, the

[4] We would like to thank the authors of ref. [53] for providing the `gg4l` code and in particular Jonas Lindert for very helpful correspondence.

JHEP01(2022)072

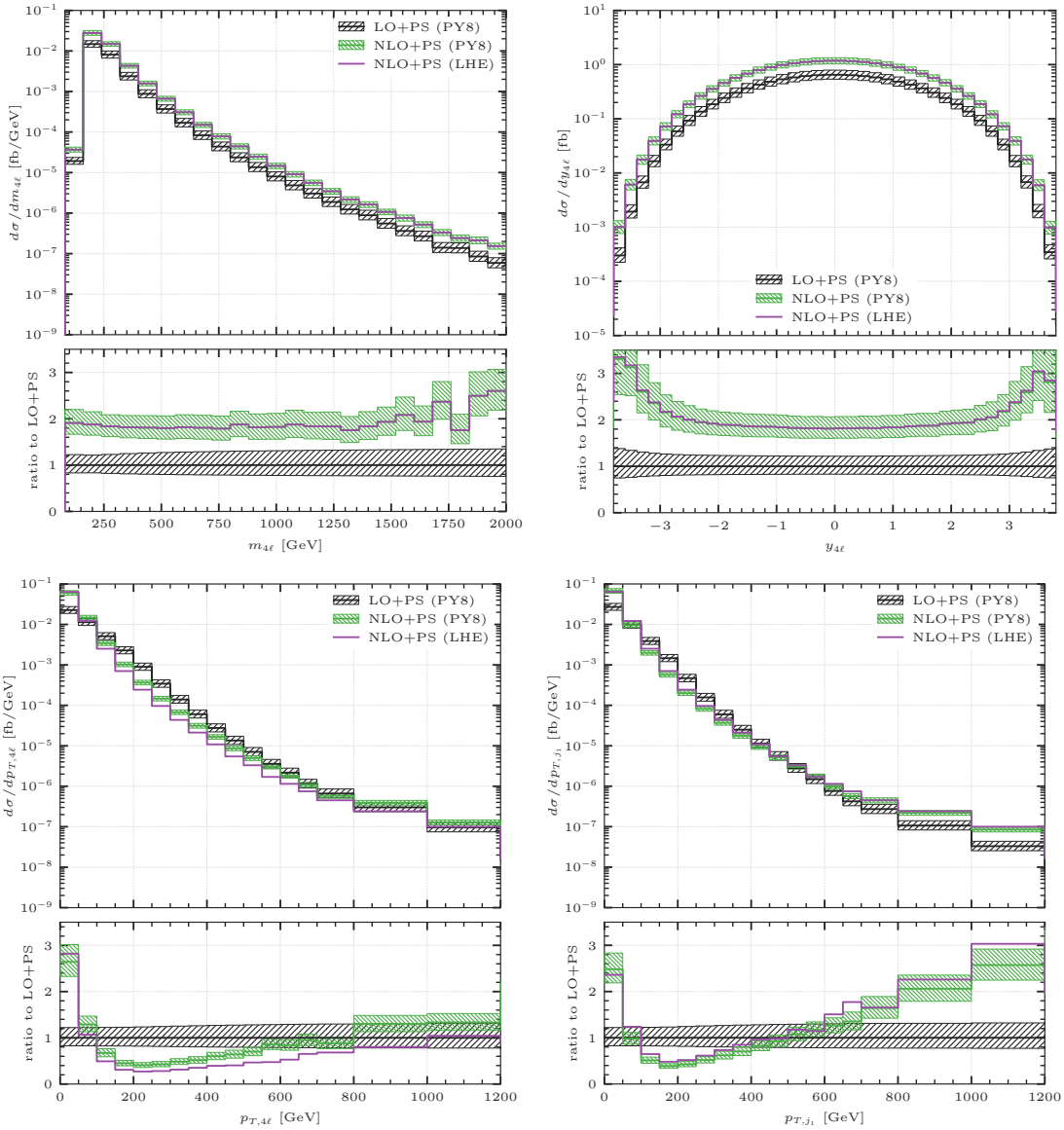

Figure 3. Predictions for ZZ production in the loop-induced gg channel at LO+PS and NLO+PS. For reference also the LHE-level central result at NLO is plotted. Shown are the distributions in the invariant mass, rapidity and transverse momentum of the four-lepton system, and in the transverse momentum of the leading jet.

uncertainty bands are obtained through a standard seven-point scale variation, and we employ the Pythia8 parton shower [129] with the A14 tune [130] (see section 3.1 for further details) to obtain the showered results presented in figure 3. For the genuine NLO-accurate quantities shown in figure 3, namely $m_{4\ell}$ and the rapidity of the four-lepton system ($y_{4\ell}$), we find results that are completely in line with the findings of previous fixed-order calculations [48, 50], which is expected since shower effects are negligible for those observables, as one can see from the LHE results. In particular, NLO corrections are sizable and increase the value of the inclusive cross section by almost a factor of two, with scale

JHEP01(2022)072

uncertainties at the level of 10-15%. In certain phase-space regions, like in the tail of the $m_{4\ell}$ distribution, the NLO corrections can even become significantly larger than a factor of two. However, in those regions the relative impact of the loop-induced gg contribution is reduced. When looking at the transverse-momentum spectrum of the four-lepton system ($p_{\mathrm{T},4\ell}$) and of the leading jet (p_{T,j_1}) in figure 3, the importance of matching to the parton shower becomes clear:[5] at LO only the parton shower fills those distributions and at NLO it still provides a substantial correction. In fact, in a fixed-order calculation both observables would diverge, and therefore be unphysical, at small transverse momenta. It is interesting to notice that the LO+PS result is actually higher than the NLO+PS one in the intermediate $p_{\mathrm{T},4\ell}$ region before it falls off steeply. This region is completely filled by the shower, whose starting scale by default is set to $m_{4\ell}$ in the LO calculation. The fact that $m_{4\ell}$ is on average relatively large explains why the shower fills the spectrum even at such high transverse momenta.

3 Phenomenological results

In this section we present phenomenological results for the process $pp \to e^+e^-\mu^+\mu^-$. After discussing our setup in section 3.1, we compare our MiNNLO$_{\mathrm{PS}}$ predictions for integrated cross sections (section 3.2) and at the differential level (section 3.3) against fixed-order predictions at NNLO accuracy, MiNLO$'$ results and experimental data from the CMS experiment [26].

3.1 Input parameters and setup

We consider proton-proton collisions at the LHC with a center-of-mass energy of 13 TeV and present predictions for $pp \to e^+e^-\mu^+\mu^-$ production. We use the complex-mass scheme [134] throughout and set the electroweak (EW) inputs to their PDG [135] values: $G_F = 1.16639 \times 10^{-5}\,\mathrm{GeV}^{-2}$, $m_W = 80.385\,\mathrm{GeV}$, $\Gamma_W = 2.0854\,\mathrm{GeV}$, $m_Z = 91.1876\,\mathrm{GeV}$, $\Gamma_Z = 2.4952\,\mathrm{GeV}$, $m_H = 125\,\mathrm{GeV}$ and $\Gamma_H = 0.00407\,\mathrm{GeV}$. We set the on-shell top-quark mass to $m_t = 173.2\,\mathrm{GeV}$, and $\Gamma_t = 1.347878\,\mathrm{GeV}$ is used. We determine the other EW parameters in the G_μ scheme with the EW coupling $\alpha_{G_\mu} = \sqrt{2}/\pi G_\mu |(m_W^2 - i\Gamma_W m_W)\sin^2\theta_W|$ and the EW mixing angle $\cos^2\theta_W = (m_W^2 - i\Gamma_W m_W)/(m_Z^2 - i\Gamma_Z m_Z)$. We use the NNPDF3.1 [27] NNLO set with $\alpha_s = 0.118$ via the LHAPDF interface [136] for all our predictions. For MiNLO$'$ and MiNNLO$_{\mathrm{PS}}$, the PDFs are read by LHAPDF and evolved internally by HOPPET [122] as described in ref. [106]. The central factorization and renormalization scales are set as discussed in section 2.2.2 for the MiNNLO$_{\mathrm{PS}}$ ZZ generator in the $q\bar{q}$ channel and as given in section 2.3 for the loop-induced gg channel. Scale uncertainties are estimated by varying μ_{F} and μ_{R} around their central value by a factor of two in each direction, while keeping the minimal and maximal values with the constraint $0.5 \leq \mu_{\mathrm{R}}/\mu_{\mathrm{F}} \leq 2$.

By combining the MiNNLO$_{\mathrm{PS}}$ $q\bar{q}$ results and loop-induced gg results at (N)LO+PS, we obtain predictions for ZZ production at (n)NNLO accuracy matched to parton showers.

[5] Note that, compared to the LO+PS results quoted for $gg \to ZZ$, predictions at higher accuracy in the presence of an additional radiated jet, possibly including zero- and one-jet merging, have been presented in refs. [131–133].

JHEP01(2022)072

	`setup-inclusive`	`setup-fiducial`
Z-mass window	$60\,\text{GeV} < m_{Z_1}, m_{Z_2} < 120\,\text{GeV}$	$60\,\text{GeV} < m_{Z_1}, m_{Z_2} < 120\,\text{GeV}$
lepton cuts	$m_{\ell^+\ell^-} > 4\,\text{GeV}$	$p_{\text{T},\ell_1} > 20\,\text{GeV}, \quad p_{\text{T},\ell_2} > 10\,\text{GeV},$ $p_{\text{T},\ell_{3,4}} > 5\,\text{GeV}, \quad \lvert\eta_\ell\rvert < 2.5,$ $m_{\ell^+\ell^-} > 4\,\text{GeV}$

Table 1. Inclusive and fiducial cuts used to the define the `setup-inclusive` and `setup-fiducial` phase space regions [26]. See text for more details.

For all (n)NNLO+PS predictions presented in this paper we make use of the Pythia8 parton shower [129] with the A14 tune [130] (`py8tune 21` in the input card). To validate our calculation and to show where shower effects are crucial, we compare (n)NNLO+PS predictions obtained with MiNNLO$_{\text{PS}}$ and (n)NNLO fixed-order predictions obtained with Matrix [115]. Additionally, we consider the inclusion of NLO EW effects. In the Matrix predictions we set $\mu_{\text{R}} = \mu_{\text{F}} = m_{4\ell}$, and we construct the scale-uncertainty bands with the same canonical seven-point scale variation used for our MiNLO$'$ and MiNNLO$_{\text{PS}}$ results.

Moreover, we compare our predictions with the most recent results by the CMS collaboration [26] within the fiducial volume defined in table 1, denoted as `setup-fiducial`. Note that the reconstructed Z bosons Z_1 and Z_2 are identified by selecting the opposite-sign same-flavour (OSSF) lepton pair with an invariant mass closest to the Z-boson mass as Z_1 and identifying the remaining OSSF lepton pair with Z_2. Since here we only consider the different-flavour channel ($e^+e^-\mu^+\mu^-$), the two Z bosons are unambiguously reconstructed and this procedure only selects which lepton pair is called Z_1 and which Z_2. Note that in the different-flavour channel the additional $m_{\ell^+\ell^-} > 4\,\text{GeV}$ cut in table 1 has no effect. Besides the fiducial setup, we also consider an inclusive setup (dubbed `setup-inclusive`), where we only require a Z-mass window between 60 GeV and 120 GeV for the two resonances.

In order to provide the most realistic comparison to experimental data, our final predictions include effects from hadronization and multi-particle interactions (MPI). We also include QED showering effects as provided by Pythia8. In order to prevent charged resonances to radiate photons and photons to branch into lepton- or quark-pairs, we set the two flags `TimeShower:QEDshowerByOther` and `TimeShower:QEDshowerByGamma` to `off`.

Finally, we define dressed leptons by adding to the four-momentum of a lepton the four-momenta of all photons within a distance $\Delta R_{\gamma\ell} = \sqrt{\Delta\phi^2_{\gamma\ell} + \Delta\eta^2_{\gamma\ell}} < 0.1$.

3.2 Integrated cross sections

We start the discussion of our results by first considering integrated cross sections. In table 2 we report predictions both in the inclusive and in the fiducial setup introduced above for various perturbative calculations. Specifically, we consider MiNLO$'$ predictions, and a number of predictions including NNLO corrections, both at fixed order and matched to parton showers through MiNNLO$_{\text{PS}}$: besides the complete NNLO predictions (that include the LO loop-induced gg contribution), we provide the NNLO corrections to the $q\bar{q}$ channel (dubbed NNLO$_{q\bar{q}}$) and nNNLO cross sections (as defined before). For completeness, we also

JHEP01(2022)072

$\sigma(pp \to e^+e^-\mu^+\mu^-)$ [fb]	`setup-inclusive`	`setup-fiducial`
NLO (MATRIX)	$32.50(1)^{+1.9\%}_{-1.6\%}$	$16.49(1)^{+1.9\%}_{-1.6\%}$
MINLO′	$31.42(3)^{+6.3\%}_{-5.0\%}$	$16.38(2)^{+6.0\%}_{-5.0\%}$
$\text{NNLO}_{q\bar{q}}$ (MATRIX)	$34.42(4)^{+1.0\%}_{-1.0\%}$	$17.45(3)^{+1.0\%}_{-1.0\%}$
NNLO (MATRIX)	$36.57(4)^{+2.4\%}_{-2.1\%}$	$18.84(3)^{+2.5\%}_{-2.1\%}$
nNNLO (MATRIX)	$38.31(4)^{+2.2\%}_{-2.0\%}$	$19.96(3)^{+2.6\%}_{-2.3\%}$
$\text{nNNLO+NLO}_{\text{EW}}$ (MATRIX)	$36.43(7)^{+2.6\%}_{-2.4\%}$	$19.00(4)^{+2.7\%}_{-2.4\%}$
$\text{nNNLO}\times\text{NLO}_{\text{EW}}$ (MATRIX)	$35.63(7)^{+2.5\%}_{-2.3\%}$	$18.58(4)^{+2.6\%}_{-2.3\%}$
$\text{NNLO}_{q\bar{q}}$+PS ($\text{MINNLO}_{\text{PS}}$)	$34.36(3)^{+0.8\%}_{-1.0\%}$	$17.45(3)^{+0.9\%}_{-1.0\%}$
NNLO+PS ($\text{MINNLO}_{\text{PS}}$)	$36.50(3)^{+1.9\%}_{-2.0\%}$	$18.90(3)^{+2.5\%}_{-2.0\%}$
nNNLO+PS ($\text{MINNLO}_{\text{PS}}$)	$38.35(3)^{+2.1\%}_{-2.0\%}$	$20.04(3)^{+2.5\%}_{-2.0\%}$
Extracted from CMS 13 TeV [26]	$39.4 \pm 0.7_{(\text{stat})}$ $\pm 1.1_{(\text{syst})} \pm 0.9_{(\text{theo})} \pm 0.7_{(\text{lumi})}$	$20.3 \pm 0.4_{(\text{stat})}$ $\pm 0.6_{(\text{syst})} \pm 0.4_{(\text{lumi})}$

Table 2. Integrated cross sections at various perturbative orders in both the `setup-inclusive` and `setup-fiducial` region. In brackets we report the statistical uncertainties, while scale uncertainties are reported in percentages. We also report the inclusive and fiducial cross sections measured by the CMS experiment in ref. [26]. Since the measured inclusive cross section corresponds to on-shell $pp \to ZZ$ production, we have multiplied the measured cross section by a branching fraction of $\text{BR}(Z \to \ell^+\ell^-) = 0.03366$, as quoted in ref. [26], for each Z boson and by a factor of two to compare with our predictions for $pp \to e^+e^-\mu^+\mu^-$ production. For the measured fiducial cross section the CMS analysis includes both different-flavour ($e^+e^-\mu^+\mu^-$) and same-flavour ($e^+e^-e^+e^-$, $\mu^+\mu^-\mu^+\mu^-$) decay channels of the two Z bosons. We have therefore divided the measured fiducial cross section by a factor of two to compare with our $pp \to e^+e^-\mu^+\mu^-$ predictions.

quote nNNLO predictions combined with NLO EW corrections, computed at fixed-order with MATRIX, either using an additive or multiplicative scheme. In the latter predictions we also take into account the photon-induced contribution at LO and beyond.[6] In order to compare our predictions to fixed-order results, all $\text{MINNLO}_{\text{PS}}$ (and MINLO′) results of table 2 are obtained at parton level, without including hadronization, MPI or photon radiation effects. We have checked explicitly that those effects have a negligible impact on the integrated cross sections.

The $\text{MINNLO}_{\text{PS}}$ prediction and the NNLO result are in excellent agreement with each other both in the inclusive and in the fiducial setup. The perturbative uncertainty at (n)NNLO(+PS) is at the 2-3% level. In particular, despite the fact that the loop-induced gg process at LO (NLO) contributes only $\sim$ 6-8% ($\sim$ 10-15%) to the NNLO (nNNLO) cross section, the uncertainties of the (n)NNLO results are dominated by the gluon-initiated contribution. The NLO correction for the loop-induced gg channel is particularly sizable, almost doubling the LO contribution entering at α_s^2, as discussed in section 2.3. Accordingly, the nNNLO central prediction is not included in the NNLO uncertainty band.

The MINLO′ result is 8-10% smaller than the $\text{MINNLO}_{\text{PS}}$ result. Its uncertainty

[6] We used the `NNPDF31_nnlo_as_0118_luxqed` [137–139] PDF set to compute fixed-order predictions which include EW corrections, and verified that the (n)NNLO prediction is modified at the few permille level with respect to the prediction obtained with `NNPDF31_nnlo_as_0118`.

JHEP01(2022)072

band, which is considerably larger than the MiNNLO$_{\rm PS}$ one, does not contain the central (n)NNLO+PS prediction, because scale variations cannot account for the additional loop-induced gg process entering at NNLO. We also note that the MiNLO$'$ uncertainty band is larger than the NLO one, and it includes the NLO result. On the contrary, the NLO uncertainty band is very small and neither MiNLO$'$ nor the NNLO central results lie inside it.

Notwithstanding the excellent agreement between the nNNLO(+PS) result and the fiducial cross section measured by CMS, the theoretical predictions should be supplemented with EW corrections. Their inclusion, using either an additive or multiplicative scheme [47], has a non-negligible impact on the nNNLO result and reduces the cross section by about 4-6% in the fiducial region, slightly deteriorating the agreement with the experimental measurement. We note that EW effects include photon-initiated processes. These have a negligible impact in the fiducial setup, where the leading lepton has a transverse momentum larger than 20 GeV, and all leptons have a transverse momentum larger than 5 GeV. On the contrary, in the inclusive setup, without a minimal transverse momentum, the photon-initiated contribution features a collinear divergence. To avoid this divergence, the CMS analysis [26] imposed a transverse momentum cut of 5 GeV on the leptons in the evaluation of the photon-induced component. With this cut, they showed that the photon-induced contribution is less than 1% of the total cross section. For this reason, we set the photon-induced component to zero for the nNNLO+NLO$_{\rm EW}$ and nNNLO×NLO$_{\rm EW}$ results in the inclusive case.

3.3 Differential distributions

In this section we present our results for differential distributions. We start by comparing the nNNLO+PS predictions obtained with MiNNLO$_{\rm PS}$ against MiNLO$'$ and fixed-order nNNLO predictions in the `setup-inclusive` in section 3.3.1. In section 3.3.2 we move to consider the `setup-fiducial` and we compare our MiNNLO$_{\rm PS}$ predictions at nNNLO+PS with the data collected and analyzed by the CMS experiment [26].

3.3.1 Comparison against theoretical predictions

In figure 4 we compare nNNLO+PS predictions for MiNNLO$_{\rm PS}$ with MiNLO$'$ and nNNLO predictions at fixed order for four different distributions which are non-zero at LO. In particular, we consider the invariant mass of the e^+e^- pair ($m_{e^+e^-}$), the invariant mass ($m_{4\ell}$) and the rapidity of the diboson system ($y_{4\ell}$), and the rapidity (y_{Z_1}) of the Z boson whose invariant mass is closer to m_Z. We remind the reader that both the MiNNLO$_{\rm PS}$ and the MiNLO$'$ predictions are obtained at parton level, without including hadronization, MPI or photon radiation effects. We observe a very good agreement between the nNNLO+PS and the nNNLO predictions, both for the central values and for the scale-variation bands. The latter are at the few-percent level across the whole range shown in the plots, becoming larger (about ±5%) at high $m_{4\ell}$. Minor differences are visible in the tails of the distributions, in particular at large $m_{4\ell}$, where the nNNLO-accurate MiNNLO$_{\rm PS}$ and fixed-order predictions however still overlap. Indeed, in the large invariant-mass region scale choices and terms beyond accuracy become increasingly important, as it was recently pointed out

JHEP01(2022)072

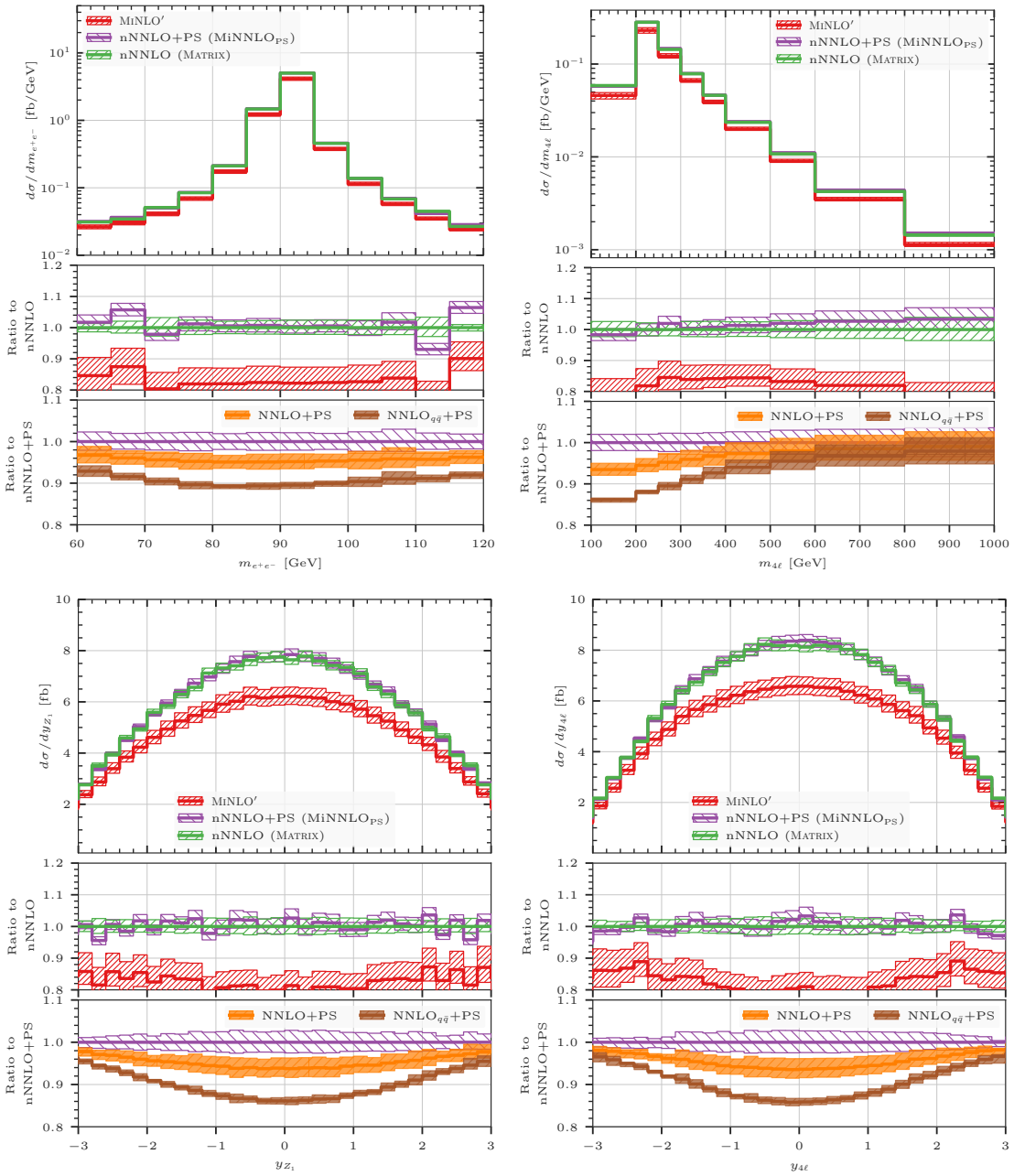

Figure 4. Comparison between selected distributions computed with Matrix, MiNNLO$_{\rm PS}$ and MiNLO′. Upper panel: invariant mass of the e^+e^- pair (left) and of the ZZ pair (right); lower panel: rapidity of Z_1 (left) and of the ZZ pair (right).

for W^+W^- production in ref. [109] and extensively discussed for $t\bar{t}$ production [140, 141]. The MiNLO′ result is in all cases about 15-20% smaller than the nNNLO results, which provides mostly flat corrections to the distributions under consideration, increasing slightly only at large $m_{4\ell}$. We stress that the relatively flat QCD corrections are a feature of the chosen distributions (in the inclusive setup) that does not apply in general, as we shall see below. Although the MiNLO′ uncertainty is a factor of 3 larger than the MiNNLO$_{\rm PS}$ and

JHEP01(2022)072

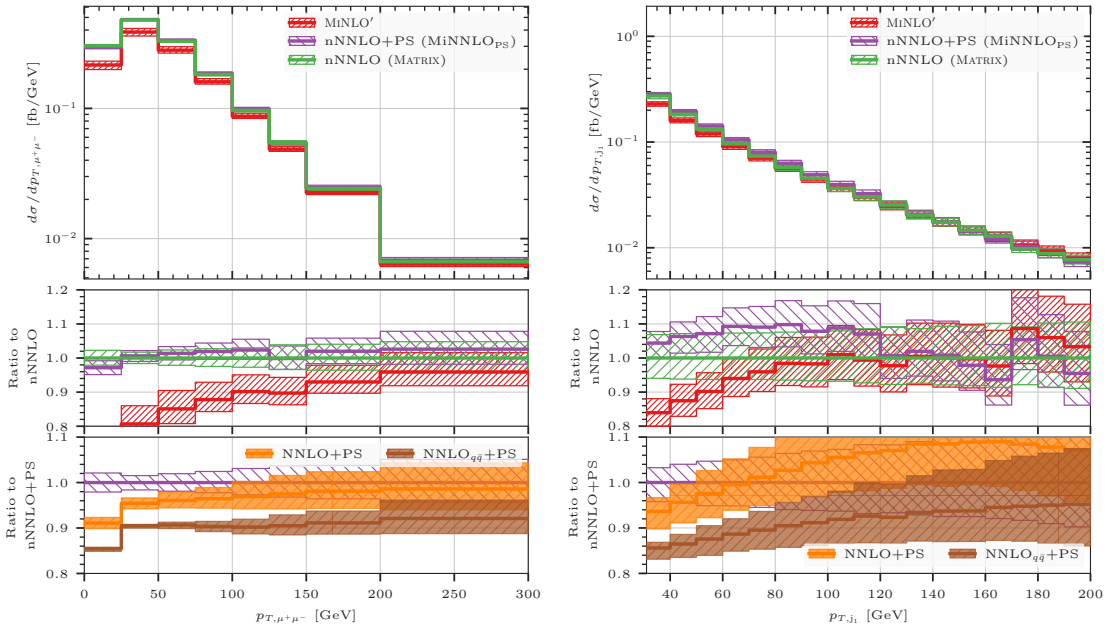

Figure 5. Same as figure 4, for the transverse momentum of the $\mu^+\mu^-$ pair (left) and of the leading jet (right).

nNNLO ones, the MiNLO′ predictions do not overlap with the nNNLO-accurate results. This is not unexpected since a large part of the difference is caused by the loop-induced gg contribution. Since the latter is missing in the MiNLO′ predictions, the MiNLO′ scale variation can not account for this new production process, which instead enters the nNNLO results. From the second ratio panel we can appreciate the effect of the loop-induced gg contribution both at LO (comparing NNLO+PS to NNLO$_{q\bar{q}}$+PS) and at NLO (comparing nNNLO+PS to NNLO$_{q\bar{q}}$+PS). It is clear from the plots that due to the gluon flux the impact of the loop-induced gg process is more prominent in certain phase-space regions. The LO (NLO) corrections, which inclusively amount to $\sim$ 6-8% ($\sim$ 10-15%) as pointed out before, contribute more significantly in the bulk region of the distributions, i.e. at the Z resonance in $m_{e^+e^-}$ as well as for small $m_{4\ell}$ and central rapidities.

In figure 5 we show the same comparison for the transverse momentum of the $\mu^+\mu^-$ pair ($p_{\mathrm{T},\mu^+\mu^-}$) and the transverse momentum of the leading jet (p_{T,j_1}) above 30 GeV. The latter was constructed using the anti-k_{T} algorithm [142] with a jet radius of $R = 0.4$ as implemented in FastJet [143]. While $p_{\mathrm{T},\mu^+\mu^-}$ is already defined at LO, p_{T,j_1} receives its first contribution only at NLO and its accuracy is thus effectively reduced by one perturbative order. The MiNNLO$_{\mathrm{PS}}$ and the nNNLO results for $p_{T,\mu^+\mu^-}$ are in good agreement with each other in the whole range shown here. The MiNLO′ result is more than 20% smaller at low values of the transverse momentum, while it agrees with the other two predictions at large values of $p_{\mathrm{T},\mu^+\mu^-}$. Hence, this distribution shows that in general QCD corrections are not uniformly distributed in phase space. By and large, the three predictions for the transverse momentum of the leading jet display a good agreement, especially in the tail of the distribution. The level of agreement between nNNLO and

JHEP01(2022)072

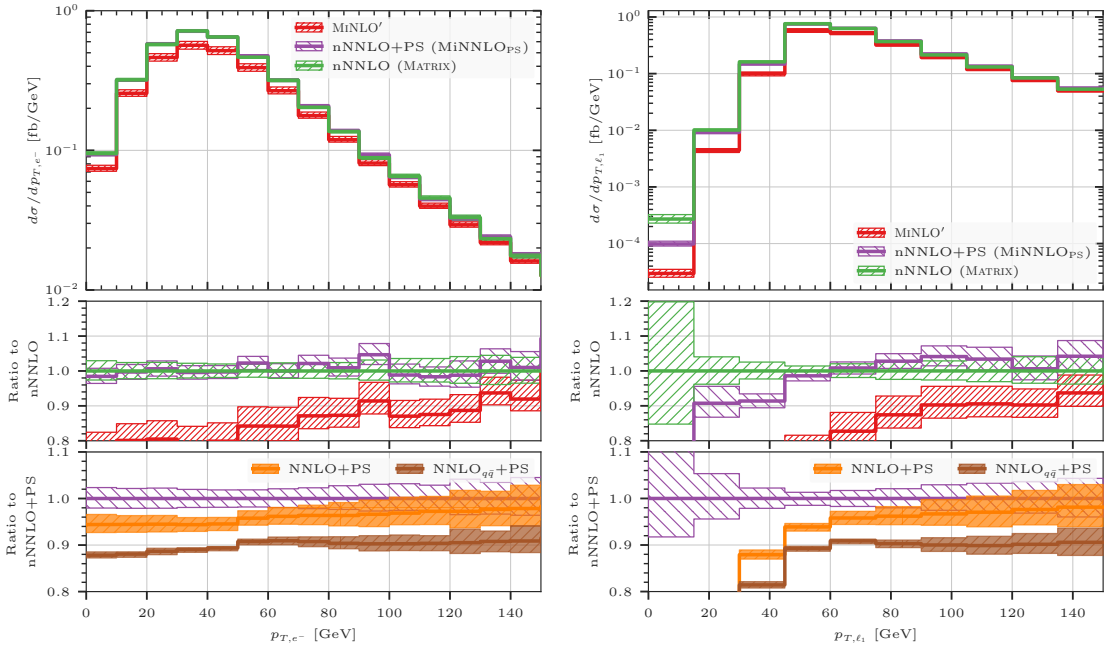

Figure 6. Same as figure 4, for the transverse momentum of the electron (left) and of the leading lepton (right).

MiNNLO$_{\rm PS}$ is expected as both predictions are effectively nNLO accurate at large $p_{{\rm T},j_1}$. The residual scale uncertainties are at the 5-10% level and they are larger than those in the other distributions, which is a direct consequence of the lower accuracy of the predictions for this distribution. Looking at the effect of loop-induced gg contribution in the second ratio panel, we observe a rather peculiar behaviour with the nNNLO+PS corrections being negative with respect to NNLO+PS for $p_{{\rm T},j_1} \gtrsim 80\,\text{GeV}$. However, this is completely in line with the results presented in figure 3 and it is a consequence of the fact that the NNLO+PS predictions include only a LO+PS calculation for the loop-induced gg process, which is not expected to describe the high $p_{{\rm T},j_1}$ range as it is filled entirely by the parton shower, which has no accuracy in this region. This further underlines the need for including NLO corrections to the loop-induced gg process. Indeed, after including the NLO corrections, the loop-induced gg contribution reduces to 5% (and less) at high $p_{{\rm T},j_1}$ (comparing nNNLO to NNLO$_{q\bar{q}}$+PS), which is more reasonable.

In figure 6 we show an analogous comparison for the transverse-momentum spectrum of the electron ($p_{{\rm T},e^-}$) and of the leading lepton ($p_{{\rm T},\ell_1}$). For the $p_{{\rm T},e^-}$ distribution we observe excellent agreement over the whole range between the MiNNLO$_{\rm PS}$ and the nNNLO results, which is fully expected since this distribution should be affected very mildly by resummation/shower effects. We have explicitly checked that a similar level of agreement is obtained when considering the same comparison at NNLO$_{q\bar{q}}$ accuracy, as opposed to the Geneva calculation in ref. [103], where differences between the Geneva and fixed-order results are observed for $p_{{\rm T},e^-} > 40\,\text{GeV}$. When comparing the MiNNLO$_{\rm PS}$ and the MiNLO′ predictions for the $p_{{\rm T},e^-}$ spectrum we observe that the effect of both the NNLO$_{q\bar{q}}$ corrections and the loop-induced gg contribution is particularly pronounced in the bulk region of the

JHEP01(2022)072

distribution, where the MiNLO′ result is more than 20% smaller than the nNNLO result. On the other hand, the transverse momentum of the leading lepton is subject to shower effects, especially at low p_{T,ℓ_1}, and indeed we observe a difference between the Matrix results and the MiNNLO$_{\mathrm{PS}}$ predictions below 40 GeV, which become increasingly larger the more steeply the distribution falls when p_{T,ℓ_1} approaches zero. Above this value, the shower effects are less pronounced and the two predictions are in good agreement. By comparing the nNNLO+PS predictions to the NNLO+PS and NNLO$_{q\bar{q}}$+PS results we can see that the impact of the loop-induced gg contribution is particularly relevant below 40 GeV, and it is also predominantly responsible for the relatively large shower effects that we observe. In fact, we have checked that for the NNLO$_{q\bar{q}}$+PS result the relative impact of the shower is smaller than for the NLO+PS result in the gg channel, which is expected considering the higher perturbative accuracy (and thereby logarithmic terms) already included at fixed order in the $q\bar{q}$ channel.

Finally, in figure 7 we show predictions for the transverse momentum of the diboson pair ($p_{T,4\ell}$). In this case, we also show the NNLO+N^{3}LL result obtained with Matrix+RadISH [144], which interfaces Matrix [115] to the RadISH resummation formalism [145, 146], using $\mu_{\mathrm{R}} = \mu_{\mathrm{F}} = m_{4\ell}$ and $Q_{\mathrm{res}} = m_{4\ell}/2$ for the resummation scale. Since Matrix+RadISH does not include the contribution stemming from the loop-induced gg channel, we perform this comparison by considering only the $q\bar{q}$-initiated process, i.e. at the NNLO$_{q\bar{q}}$(+PS) level. At small values of the ZZ transverse momentum we observe an excellent agreement between the NNLO+N^{3}LL and the MiNNLO$_{\mathrm{PS}}$ result, especially considering the lower accuracy of the parton shower in that region; MiNNLO$_{\mathrm{PS}}$ is between 5% and 8% larger than the NNLO+N^{3}LL prediction below 10 GeV and has a larger uncertainty band reflecting its lower accuracy. On the other hand, the MiNLO′ result is $\mathcal{O}(10\%)$ smaller than the NNLO+N^{3}LL and the MiNNLO$_{\mathrm{PS}}$ predictions and its uncertainty band does not overlap with either of the more accurate results below 40 GeV. Fixed-order calculations actually lead to unphysical results in the small-$p_{\mathrm{T},4\ell}$ region due to large logarithmic corrections, which need to be resummed to all orders. Indeed, the NNLO result diverges at low transverse momentum, and its prediction differs significantly from the ones including resummation effects. At larger values of $p_{\mathrm{T},4\ell}$ the NNLO result is instead in agreement with the NNLO+N^{3}LL, MiNLO′ and MiNNLO$_{\mathrm{PS}}$ predictions, as one may expect since all of them have the same formal accuracy in the tail of the distribution.

In conclusion, we observe overall a very good agreement between MiNNLO$_{\mathrm{PS}}$, fixed-order, and analytically resummed results across a variety of distributions, which provides a robust validation of our calculation. The MiNLO′ result, despite the considerably larger uncertainty bands, rarely overlaps with the (n)NNLO(+PS) predictions, thus highlighting the importance of higher-order corrections to this process. Moreover, certain observables require the resummation of large logarithmic contributions, which renders the matching to the parton shower mandatory.

3.3.2 Comparison against data

In this section we compare our MiNNLO$_{\mathrm{PS}}$ predictions at nNNLO+PS to the CMS measurement presented in ref. [26] in the `setup-fiducial` defined in table 1. We have gener-

JHEP01(2022)072

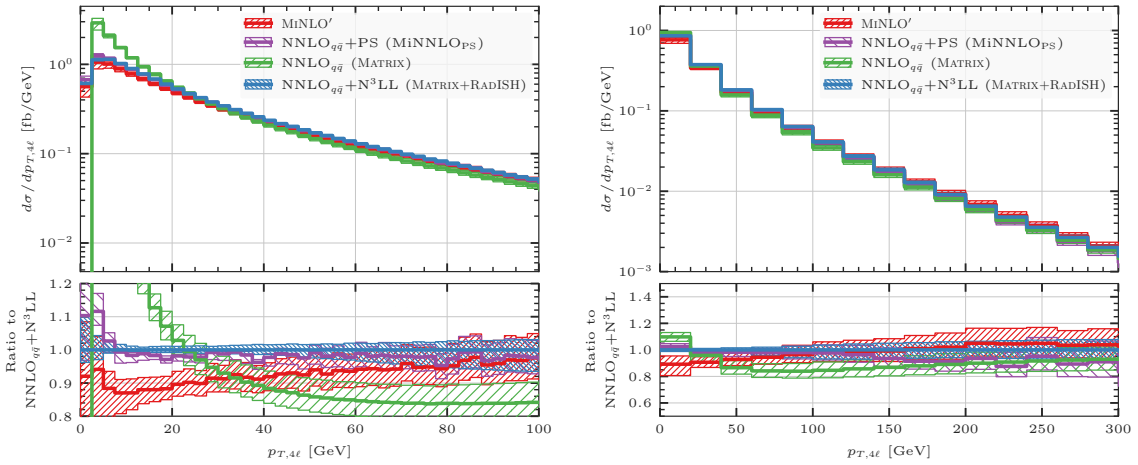

Figure 7. Same as figure 4, for the transverse momentum of the ZZ pair for two different ranges of $p_{T,4\ell}$. In both plots, we also show the NNLO+N^{3}LL result computed with Matrix+RadISH [144].

ated the events and estimated the theoretical uncertainties as described in section 3.1. We note that in order to compare against data our predictions include MPI and hadronization effects, as well as QED corrections in the shower approximation.

The comparison between MiNNLOPS predictions and experimental data is presented in figure 8. Altogether, we show predictions for six observables: the invariant mass and the transverse momentum of the diboson pair ($m_{4\ell}$ and $p_{\mathrm{T},4\ell}$), the sum of the four individual transverse-momentum distributions of each final-state lepton (which corresponds to the average of the lepton transverse-momentum distributions), the sum of the two distributions of the transverse momentum of the reconstructed Z bosons (which analogously corresponds to the average of the Z transverse-momentum distributions), and the separation between the two Z bosons in the azimuthal angle ($\Delta\phi_{Z_1,Z_2}$) and in the η–ϕ plane ($\Delta R_{Z_1,Z_2}$). In all cases, except for $\Delta\phi_{Z_1,Z_2}$ that has a kinematical endpoint at $\Delta\phi = \pi$, the last bin shown in the figures also includes the contribution of the overflow.

By and large, we observe a quite remarkable agreement between our predictions and the experimental data. The invariant mass is well described at low $m_{4\ell}$, but there is a tendency of the data to undershoot the prediction at large $m_{4\ell}$, with the last bin being almost two standard deviations away. In this region EW corrections are known to be important and they are only partly included here through the QED shower. Below, we discuss how the inclusion of the NLO EW corrections at fixed order improves the agreement with data in this region. The transverse-momentum distribution of the ZZ pair is also well described, except for a two-sigma deviation in the last bin, with a remarkable agreement for $p_{\mathrm{T},4\ell}$ values below $\sim 100\,\mathrm{GeV}$, where the all-order corrections provided by the shower are particularly important. The two averaged distributions of p_{T,ℓ_i} and p_{T,Z_i} also compare very well to MiNNLOPS, with deviations in the tail of the distributions only. In the last bins the experimental data are about two standard deviations away from the theoretical predictions, which can again be related to the missing EW corrections, as discussed below. The $\Delta\phi_{Z_1,Z_2}$ and the $\Delta R_{Z_1,Z_2}$ distributions are also very well described by MiNNLOPS,

JHEP01(2022)072

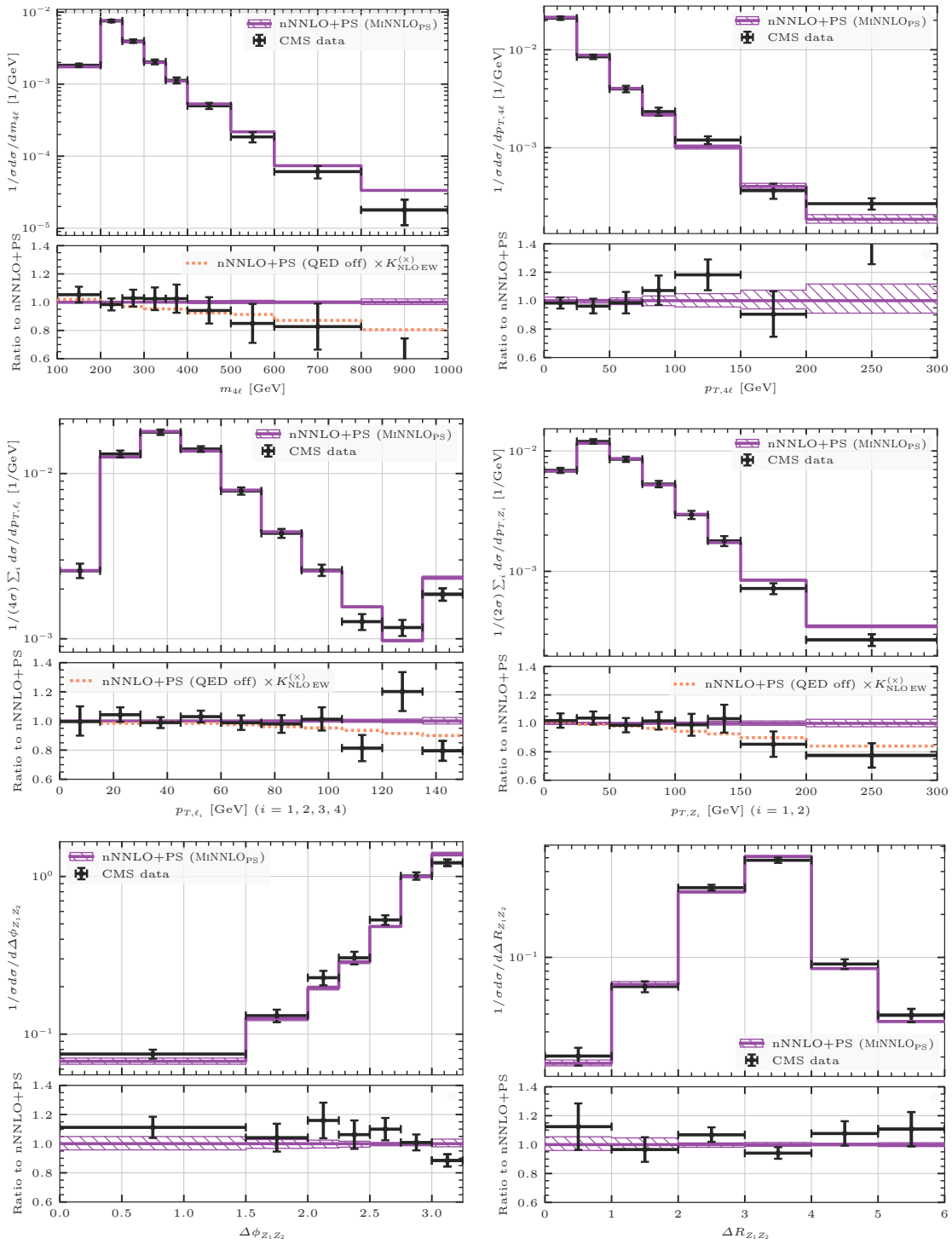

Figure 8. Comparison between the MiNNLO$_{\mathrm{PS}}$ predictions and the CMS data of ref. [26] based on a 137 fb^{-1} 13 TeV analysis for various observables. The MiNNLO$_{\mathrm{PS}}$ predictions include hadronization and MPI effects, as well as QED effects as provided by the Pythia8 parton shower. See text for more details.

JHEP01(2022)072

with the data fluctuating (within one sigma, except for one bin with a two-sigma deviation) around the central theoretical prediction across the whole plotted range.

The comparison at the level of integrated cross section in section 3.2 showed that the inclusion of NLO EW effects has a small, but non-negligible impact in the fiducial setup. Since in our comparison with data we include QED effects via parton-shower matching, one may wonder whether the proper inclusion of NLO EW effects in a Monte Carlo context, see e.g. refs. [41, 147], would further improve the agreement with the data, especially in the tails of distributions where EW logarithms are important. A possible way to assess the impact of the EW corrections beyond the parton shower approximation is to apply to the MiNNLO$_{\rm PS}$ predictions a differential K-factor correction for the NLO EW corrections that is computed at fixed order accuracy.

We have done this exercise turning off the QED shower in the MiNNLO$_{\rm PS}$ predictions to avoid double counting. The central rescaled prediction is shown in the lower ratio panels in figure 8. We adopt as our default a factor $K^{(\times)}_{\rm NLOEW}$, defined using the multiplicative scheme nNNLO$\times$NLO$_{\rm EW}$ [47], which includes an estimate of mixed higher-order corrections, divided by the nNNLO result. Note that for distributions starting at NLO QCD we do not perform this additional comparison, since one would need to compute the EW corrections to the ZZ+1-jet process. We find that the inclusion of NLO EW corrections within this approximation improves the agreement with the experimental data for the tails of the $m_{4\ell}$ and the averaged $p_{{\rm T},Z_i}$ distributions, where the effects of Sudakov logarithms are expected to be visible. For the averaged $p_{{\rm T},\ell_i}$ distribution their impact is a bit milder, also because the distribution extends to lower values, and there is no significant improvement compared to data. Furthermore, we would like to add some comments on the effects of the QED shower below the $m_{4\ell} \sim 2\,m_Z$ threshold (where QED effects are expected to be sizable) in light of its limited accuracy. First of all, we verified that its effect is below 10% in the first bin of the $m_{4\ell}$ distribution in figure 8, but it can become as large as 35% when considering the `setup-inclusive` for the same bin instead. Moreover, we notice from figure 8 that the approximation of the QED shower in that region is in good agreement with the result including NLO EW effects. This is not unexpected, because logarithmic contributions due to EW Sudakov effects are small in that region and the first emission is the most relevant one for dressed leptons. We leave a consistent inclusion of NLO EW effects in our MiNNLO$_{\rm PS}$ predictions with a complete and consistent matching to QCD and QED showers to future work.

4 Conclusions

In this work, we have advanced the state of the art for Monte Carlo simulations of Z-boson pair production at the LHC. For the $q\bar{q}$-initiated process we have matched NNLO QCD predictions to parton showers using the MiNNLO$_{\rm PS}$ method. We have furthermore included the loop-induced gg-initiated process, which contributes at $\mathcal{O}(\alpha_s^2)$, in the Powheg-Box-Res framework at NLO QCD accuracy matched to parton showers. When combined, the ensuing nNNLO+PS results constitute the most accurate theoretical predictions for this process to date. We remind the reader that the benefits of the MiNNLO$_{\rm PS}$

JHEP01(2022)072

approach reside in (1) the possibility to include NNLO corrections on-the-fly, without the need of any a-posteriori reweighting, (2) the absence of any merging scale or unphysical boundaries to partition the phase space into different regions according to the number of resolved emissions, and (3) the fact that the logarithmic accuracy of the parton shower is preserved by the matching (when using a $p_{\rm T}$-ordered shower). We stress that this last feature is in general far from trivial.

We have performed an extensive comparison of our MiNNLO$_{\rm PS}$ predictions against (n)NNLO fixed-order results and the analytic resummation in the transverse momentum of the four-lepton system. We found excellent agreement with fixed-order predictions in phase-space regions where shower effects are expected to be small. As expected, for distributions that have a singularity at fixed order the MiNNLO$_{\rm PS}$ predictions feature the appropriate Sudakov damping close to the singularity and yield physical results. In particular, the comparison to the NNLO+N^{3}LL $p_{{\rm T},4\ell}$ spectrum showed quite a remarkable agreement. Moreover, we have shown that MiNNLO$_{\rm PS}$ corrections are at the level of 15-20% with respect to MiNLO$'$, and that the matching to the parton shower is crucial for observables sensitive to soft-gluon effects. It is interesting to notice that we do not observe the mild tension in the $p_{{\rm T},e^-}$ distribution observed in ref. [103] when comparing NNLO$_{q\bar{q}}$+PS to fixed-order predictions, which motivates a more comprehensive comparison between Geneva and MiNNLO$_{\rm PS}$ predictions in the future.

We have compared our nNNLO+PS predictions against 13 TeV CMS data of ref. [26] and found excellent agreement both at the level of production rates and shapes of kinematical distributions, with nNNLO+PS predictions and CMS data agreeing on almost all bins within one sigma. In the few bins where the differences are at the two-sigma level we have shown that the inclusion of NLO EW corrections removes those differences in most instances. Our final results have missing higher-order uncertainties that are of the order of 2% both for inclusive and fiducial cross sections. These uncertainties[7] are of similar size as the current precision of experimental results, which will further decrease in the future. It is then clear that theoretical predictions with an accuracy comparable to that of the results presented in this paper are mandatory to fully exploit ZZ cross section measurements at the LHC. This is particularly the case when using ZZ production data for off-shell Higgs cross section measurements in the $H \to 4\ell$ channel to put bounds on the Higgs-boson width, or when constraining the coefficients of effective-field-theory operators or anomalous triple-gauge couplings. It is interesting to note that, even though the loop-induced gg contribution is only about 10% of the total cross section, its uncertainty dominates our final predictions. It is unlikely that a three-loop calculation for this process will become available in the near future. Still, the theoretical precision can be further improved if one imposes fiducial cuts that suppress the loop-induced gluon fusion contribution. For instance, when requiring a large invariant mass of the lepton system or when considering high-$p_{\rm T}$ leptons, as done in BSM searches, the gluon-fusion contribution becomes less important since the

[7] We note that we consider here only uncertainties associated to scale variation. In particular we have omitted PDF uncertainties, those related to missing interference effects in the case of identical leptons in the final state, and those intrinsic to the approximations in the event simulation (e.g. related to the QED shower).

JHEP01(2022)072

gluon PDFs decrease strongly at large x values. On the other hand, electroweak effects become more important in these regions. The approximate combination considered here, which already increases the agreement with the experimental data in the high-energy tails, needs to be improved by combining highest-order QCD and QED corrections consistently in parton-shower simulations in the future.

Since the evaluation of the two-loop contributions is numerically highly demanding, we made full use of the reweighting facility of POWHEG and introduced the possibility to evaluate the two-loop contributions only at the very end of the event generation, considerably speeding up the calculation. The code used for our simulations will be soon made publicly available within POWHEG-BOX-RES. We are confident that this will be valuable for upcoming experimental measurements of ZZ production at the LHC, which require an accurate and fully exclusive simulation of hadron-level events, including all-order, non-perturbative, and QED effects.

Acknowledgments

We are grateful to Stefano Forte, Pier Francesco Monni, Paolo Nason and Emanuele Re for various fruitful discussions. We thank the authors of ref. [53] for providing the `gg4l` code and especially Jonas Lindert for very helpful communication. We have used the Max Planck Computing and Data Facility (MPCDF) in Garching and the cloud-computing facilities of the group of Massimiliano Grazzini at the University of Zurich to carry out the simulations related to this work. LB and LR are supported by the Swiss National Science Foundation (SNF) under contract 200020_188464.

References

[1] F. Caola and K. Melnikov, *Constraining the Higgs boson width with ZZ production at the LHC*, *Phys. Rev. D* **88** (2013) 054024 [arXiv:1307.4935] [INSPIRE].

[2] J.M. Campbell, R.K. Ellis and C. Williams, *Bounding the Higgs Width at the LHC using full analytic results for $gg \to e^-e^+\mu^-\mu^+$*, *JHEP* **04** (2014) 060 [arXiv:1311.3589] [INSPIRE].

[3] J.M. Campbell, R.K. Ellis and C. Williams, *Bounding the Higgs width at the LHC: complementary results from $H \to WW$*, *Phys. Rev. D* **89** (2014) 053011 [arXiv:1312.1628] [INSPIRE].

[4] J.M. Campbell, R.K. Ellis and C. Williams, *Bounding the Higgs Width at the LHC*, PoS(LL2014)008 [arXiv:1408.1723] [INSPIRE].

[5] M. Grazzini, S. Kallweit, M. Wiesemann and J.Y. Yook, *Four lepton production in gluon fusion: Off-shell Higgs effects in NLO QCD*, *Phys. Lett. B* **819** (2021) 136465 [arXiv:2102.08344] [INSPIRE].

JHEP01(2022)072

[6] CMS collaboration, *Constraints on the Higgs boson width from off-shell production and decay to Z-boson pairs*, *Phys. Lett. B* **736** (2014) 64 [arXiv:1405.3455] [INSPIRE].

[7] ATLAS collaboration, *Constraints on the off-shell Higgs boson signal strength in the high-mass ZZ and WW final states with the ATLAS detector*, *Eur. Phys. J. C* **75** (2015) 335 [arXiv:1503.01060] [INSPIRE].

[8] CMS collaboration, *Limits on the Higgs boson lifetime and width from its decay to four charged leptons*, *Phys. Rev. D* **92** (2015) 072010 [arXiv:1507.06656] [INSPIRE].

[9] CMS collaboration, *Search for Higgs boson off-shell production in proton-proton collisions at 7 and 8 TeV and derivation of constraints on its total decay width*, *JHEP* **09** (2016) 051 [arXiv:1605.02329] [INSPIRE].

[10] ATLAS collaboration, *Constraints on off-shell Higgs boson production and the Higgs boson total width in $ZZ \to 4\ell$ and $ZZ \to 2\ell 2\nu$ final states with the ATLAS detector*, *Phys. Lett. B* **786** (2018) 223 [arXiv:1808.01191] [INSPIRE].

[11] CMS collaboration, *Measurements of the Higgs boson width and anomalous HVV couplings from on-shell and off-shell production in the four-lepton final state*, *Phys. Rev. D* **99** (2019) 112003 [arXiv:1901.00174] [INSPIRE].

[12] CMS collaboration, *Measurements of the electroweak diboson production cross sections in proton-proton collisions at $\sqrt{s} = 5.02$ TeV using leptonic decays*, *Phys. Rev. Lett.* **127** (2021) 191801 [arXiv:2107.01137] [INSPIRE].

[13] ATLAS collaboration, *Measurement of the ZZ production cross section and limits on anomalous neutral triple gauge couplings in proton-proton collisions at $\sqrt{s} = 7$ TeV with the ATLAS detector*, *Phys. Rev. Lett.* **108** (2012) 041804 [arXiv:1110.5016] [INSPIRE].

[14] ATLAS collaboration, *Measurement of ZZ production in pp collisions at $\sqrt{s} = 7$ TeV and limits on anomalous ZZZ and $ZZ\gamma$ couplings with the ATLAS detector*, *JHEP* **03** (2013) 128 [arXiv:1211.6096] [INSPIRE].

[15] CMS collaboration, *Measurement of the ZZ production cross section and search for anomalous couplings in $2l2l'$ final states in pp collisions at $\sqrt{s} = 7$ TeV*, *JHEP* **01** (2013) 063 [arXiv:1211.4890] [INSPIRE].

[16] CMS collaboration, *Measurements of the ZZ production cross sections in the $2l2\nu$ channel in proton-proton collisions at $\sqrt{s} = 7$ and 8 TeV and combined constraints on triple gauge couplings*, *Eur. Phys. J. C* **75** (2015) 511 [arXiv:1503.05467] [INSPIRE].

[17] CMS collaboration, *Measurement of W^+W^- and ZZ production cross sections in pp collisions at $\sqrt{s} = 8TeV$*, *Phys. Lett. B* **721** (2013) 190 [arXiv:1301.4698] [INSPIRE].

[18] CMS collaboration, *Measurement of the $pp \to Zz$ production cross section and constraints on anomalous triple gauge couplings in four-lepton final states at $\sqrt{s} = 8$ TeV*, *Phys. Lett. B* **740** (2015) 250 [*Erratum ibid.* **757** (2016) 569] [arXiv:1406.0113] [INSPIRE].

[19] ATLAS collaboration, *Measurements of four-lepton production in pp collisions at $\sqrt{s} = 8$ TeV with the ATLAS detector*, *Phys. Lett. B* **753** (2016) 552 [arXiv:1509.07844] [INSPIRE].

[20] ATLAS collaboration, *Measurement of the ZZ production cross section in proton-proton collisions at $\sqrt{s} = 8$ TeV using the $ZZ \to \ell^-\ell^+\ell'^-\ell'^+$ and $ZZ \to \ell^-\ell^+\nu\bar{\nu}$ channels with the ATLAS detector*, *JHEP* **01** (2017) 099 [arXiv:1610.07585] [INSPIRE].

[21] CMS collaboration, *Measurement of differential cross sections for Z boson pair production in association with jets at $\sqrt{s} = 8$ and 13 TeV*, *Phys. Lett. B* **789** (2019) 19 [arXiv:1806.11073] [INSPIRE].

JHEP01(2022)072

[22] CMS collaboration, *Measurement of the ZZ production cross section and $Z \to \ell^+\ell^-\ell'^+\ell'^-$ branching fraction in pp collisions at $\sqrt{s} = 13$ TeV*, *Phys. Lett. B* **763** (2016) 280 [*Erratum ibid.* **772** (2017) 884] [arXiv:1607.08834] [INSPIRE].

[23] ATLAS collaboration, *$ZZ \to \ell^+\ell^-\ell'^+\ell'^-$ cross-section measurements and search for anomalous triple gauge couplings in 13 TeV pp collisions with the ATLAS detector*, *Phys. Rev. D* **97** (2018) 032005 [arXiv:1709.07703] [INSPIRE].

[24] CMS collaboration, *Measurements of the $pp \to ZZ$ production cross section and the $Z \to 4\ell$ branching fraction, and constraints on anomalous triple gauge couplings at $\sqrt{s} = 13$ TeV*, *Eur. Phys. J. C* **78** (2018) 165 [*Erratum ibid.* **78** (2018) 515] [arXiv:1709.08601] [INSPIRE].

[25] ATLAS collaboration, *Measurement of ZZ production in the $\ell\ell\nu\nu$ final state with the ATLAS detector in pp collisions at $\sqrt{s} = 13$ TeV*, *JHEP* **10** (2019) 127 [arXiv:1905.07163] [INSPIRE].

[26] CMS collaboration, *Measurements of $pp \to ZZ$ production cross sections and constraints on anomalous triple gauge couplings at $\sqrt{s} = 13$ TeV*, *Eur. Phys. J. C* **81** (2021) 200 [arXiv:2009.01186] [INSPIRE].

[27] NNPDF collaboration, *Parton distributions from high-precision collider data*, *Eur. Phys. J. C* **77** (2017) 663 [arXiv:1706.00428] [INSPIRE].

[28] B. Mele, P. Nason and G. Ridolfi, *QCD radiative corrections to Z boson pair production in hadronic collisions*, *Nucl. Phys. B* **357** (1991) 409 [INSPIRE].

[29] J. Ohnemus and J.F. Owens, *An order α^-s calculation of hadronic ZZ production*, *Phys. Rev. D* **43** (1991) 3626 [INSPIRE].

[30] J. Ohnemus, *Hadronic ZZ, W^-W^+, and $W^\pm Z$ production with QCD corrections and leptonic decays*, *Phys. Rev. D* **50** (1994) 1931 [hep-ph/9403331] [INSPIRE].

[31] L.J. Dixon, Z. Kunszt and A. Signer, *Helicity amplitudes for $O(\alpha_s)$ production of W^+W^-, $W^\pm Z$, ZZ, $W^\pm\gamma$, or $Z\gamma$ pairs at hadron colliders*, *Nucl. Phys. B* **531** (1998) 3 [hep-ph/9803250] [INSPIRE].

[32] J.M. Campbell and R.K. Ellis, *An update on vector boson pair production at hadron colliders*, *Phys. Rev. D* **60** (1999) 113006 [hep-ph/9905386] [INSPIRE].

[33] T. Melia, P. Nason, R. Rontsch and G. Zanderighi, *W^+W^-, WZ and ZZ production in the POWHEG BOX*, *JHEP* **11** (2011) 078 [arXiv:1107.5051] [INSPIRE].

[34] P. Nason and G. Zanderighi, *W^+W^- , WZ and ZZ production in the POWHEG-BOX-V2*, *Eur. Phys. J. C* **74** (2014) 2702 [arXiv:1311.1365] [INSPIRE].

[35] R. Frederix, S. Frixione, V. Hirschi, F. Maltoni, R. Pittau and P. Torrielli, *Four-lepton production at hadron colliders: aMC@NLO predictions with theoretical uncertainties*, *JHEP* **02** (2012) 099 [arXiv:1110.4738] [INSPIRE].

[36] A. Bierweiler, T. Kasprzik and J.H. Kühn, *Vector-boson pair production at the LHC to $\mathcal{O}(\alpha^3)$ accuracy*, *JHEP* **12** (2013) 071 [arXiv:1305.5402] [INSPIRE].

[37] J. Baglio, L.D. Ninh and M.M. Weber, *Massive gauge boson pair production at the LHC: a next-to-leading order story*, *Phys. Rev. D* **88** (2013) 113005 [*Erratum ibid.* **94** (2016) 099902] [arXiv:1307.4331] [INSPIRE].

[38] B. Biedermann, A. Denner, S. Dittmaier, L. Hofer and B. Jäger, *Electroweak corrections to $pp \to \mu^+\mu^-e^+e^- + X$ at the LHC: a Higgs background study*, *Phys. Rev. Lett.* **116** (2016) 161803 [arXiv:1601.07787] [INSPIRE].

JHEP01(2022)072

[39] B. Biedermann, A. Denner, S. Dittmaier, L. Hofer and B. Jager, *Next-to-leading-order electroweak corrections to the production of four charged leptons at the LHC*, *JHEP* **01** (2017) 033 [arXiv:1611.05338] [INSPIRE].

[40] M. Chiesa, A. Denner and J.-N. Lang, *Anomalous triple-gauge-boson interactions in vector-boson pair production with RECOLA2*, *Eur. Phys. J. C* **78** (2018) 467 [arXiv:1804.01477] [INSPIRE].

[41] M. Chiesa, C. Oleari and E. Re, *NLO QCD+NLO EW corrections to diboson production matched to parton shower*, *Eur. Phys. J. C* **80** (2020) 849 [arXiv:2005.12146] [INSPIRE].

[42] A. Denner and G. Pelliccioli, *NLO EW and QCD corrections to polarized ZZ production in the four-charged-lepton channel at the LHC*, *JHEP* **10** (2021) 097 [arXiv:2107.06579] [INSPIRE].

[43] F. Cascioli et al., *ZZ production at hadron colliders in NNLO QCD*, *Phys. Lett. B* **735** (2014) 311 [arXiv:1405.2219] [INSPIRE].

[44] G. Heinrich, S. Jahn, S.P. Jones, M. Kerner and J. Pires, *NNLO predictions for Z-boson pair production at the LHC*, *JHEP* **03** (2018) 142 [arXiv:1710.06294] [INSPIRE].

[45] M. Grazzini, S. Kallweit and D. Rathlev, *ZZ production at the LHC: fiducial cross sections and distributions in NNLO QCD*, *Phys. Lett. B* **750** (2015) 407 [arXiv:1507.06257] [INSPIRE].

[46] S. Kallweit and M. Wiesemann, *ZZ production at the LHC: NNLO predictions for $2\ell 2\nu$ and 4ℓ signatures*, *Phys. Lett. B* **786** (2018) 382 [arXiv:1806.05941] [INSPIRE].

[47] M. Grazzini, S. Kallweit, J.M. Lindert, S. Pozzorini and M. Wiesemann, *NNLO QCD + NLO EW with Matrix+OpenLoops: precise predictions for vector-boson pair production*, *JHEP* **02** (2020) 087 [arXiv:1912.00068] [INSPIRE].

[48] F. Caola, K. Melnikov, R. Röntsch and L. Tancredi, *QCD corrections to ZZ production in gluon fusion at the LHC*, *Phys. Rev. D* **92** (2015) 094028 [arXiv:1509.06734] [INSPIRE].

[49] F. Caola, M. Dowling, K. Melnikov, R. Röntsch and L. Tancredi, *QCD corrections to vector boson pair production in gluon fusion including interference effects with off-shell Higgs at the LHC*, *JHEP* **07** (2016) 087 [arXiv:1605.04610] [INSPIRE].

[50] M. Grazzini, S. Kallweit, M. Wiesemann and J.Y. Yook, *ZZ production at the LHC: NLO QCD corrections to the loop-induced gluon fusion channel*, *JHEP* **03** (2019) 070 [arXiv:1811.09593] [INSPIRE].

[51] T. Binoth, N. Kauer and P. Mertsch, *Gluon-induced QCD corrections to $pp \to ZZ \to l\bar{l}l'\bar{l}^{-\prime}$*, arXiv:0807.0024 [INSPIRE].

[52] S. Alioli, F. Caola, G. Luisoni and R. Röntsch, *ZZ production in gluon fusion at NLO matched to parton-shower*, *Phys. Rev. D* **95** (2017) 034042 [arXiv:1609.09719] [INSPIRE].

[53] S. Alioli, S. Ferrario Ravasio, J.M. Lindert and R. Röntsch, *Four-lepton production in gluon fusion at NLO matched to parton showers*, *Eur. Phys. J. C* **81** (2021) 687 [arXiv:2102.07783] [INSPIRE].

[54] G. Ferrera, M. Grazzini and F. Tramontano, *Associated WH production at hadron colliders: a fully exclusive QCD calculation at NNLO*, *Phys. Rev. Lett.* **107** (2011) 152003 [arXiv:1107.1164] [INSPIRE].

[55] G. Ferrera, M. Grazzini and F. Tramontano, *Associated ZH production at hadron colliders: the fully differential NNLO QCD calculation*, *Phys. Lett. B* **740** (2015) 51 [arXiv:1407.4747] [INSPIRE].

JHEP01(2022)072

[56] G. Ferrera, G. Somogyi and F. Tramontano, *Associated production of a Higgs boson decaying into bottom quarks at the LHC in full NNLO QCD*, *Phys. Lett. B* **780** (2018) 346 [arXiv:1705.10304] [INSPIRE].

[57] J.M. Campbell, R.K. Ellis and C. Williams, *Associated production of a Higgs boson at NNLO*, *JHEP* **06** (2016) 179 [arXiv:1601.00658] [INSPIRE].

[58] R.V. Harlander and W.B. Kilgore, *Higgs boson production in bottom quark fusion at next-to-next-to leading order*, *Phys. Rev. D* **68** (2003) 013001 [hep-ph/0304035] [INSPIRE].

[59] R.V. Harlander, K.J. Ozeren and M. Wiesemann, *Higgs plus jet production in bottom quark annihilation at next-to-leading order*, *Phys. Lett. B* **693** (2010) 269 [arXiv:1007.5411] [INSPIRE].

[60] R. Harlander and M. Wiesemann, *Jet-veto in bottom-quark induced Higgs production at next-to-next-to-leading order*, *JHEP* **04** (2012) 066 [arXiv:1111.2182] [INSPIRE].

[61] S. Bühler, F. Herzog, A. Lazopoulos and R. Müller, *The fully differential hadronic production of a Higgs boson via bottom quark fusion at NNLO*, *JHEP* **07** (2012) 115 [arXiv:1204.4415] [INSPIRE].

[62] S. Marzani, R.D. Ball, V. Del Duca, S. Forte and A. Vicini, *Higgs production via gluon-gluon fusion with finite top mass beyond next-to-leading order*, *Nucl. Phys. B* **800** (2008) 127 [arXiv:0801.2544] [INSPIRE].

[63] R.V. Harlander and K.J. Ozeren, *Finite top mass effects for hadronic Higgs production at next-to-next-to-leading order*, *JHEP* **11** (2009) 088 [arXiv:0909.3420] [INSPIRE].

[64] R.V. Harlander, H. Mantler, S. Marzani and K.J. Ozeren, *Higgs production in gluon fusion at next-to-next-to-leading order QCD for finite top mass*, *Eur. Phys. J. C* **66** (2010) 359 [arXiv:0912.2104] [INSPIRE].

[65] A. Pak, M. Rogal and M. Steinhauser, *Finite top quark mass effects in NNLO Higgs boson production at LHC*, *JHEP* **02** (2010) 025 [arXiv:0911.4662] [INSPIRE].

[66] T. Neumann and M. Wiesemann, *Finite top-mass effects in gluon-induced Higgs production with a jet-veto at NNLO*, *JHEP* **11** (2014) 150 [arXiv:1408.6836] [INSPIRE].

[67] S. Catani, L. Cieri, D. de Florian, G. Ferrera and M. Grazzini, *Diphoton production at hadron colliders: a fully-differential QCD calculation at NNLO*, *Phys. Rev. Lett.* **108** (2012) 072001 [*Erratum ibid.* **117** (2016) 089901] [arXiv:1110.2375] [INSPIRE].

[68] J.M. Campbell, R.K. Ellis, Y. Li and C. Williams, *Predictions for diphoton production at the LHC through NNLO in QCD*, *JHEP* **07** (2016) 148 [arXiv:1603.02663] [INSPIRE].

[69] M. Grazzini, S. Kallweit, D. Rathlev and A. Torre, *$Z\gamma$ production at hadron colliders in NNLO QCD*, *Phys. Lett. B* **731** (2014) 204 [arXiv:1309.7000] [INSPIRE].

[70] M. Grazzini, S. Kallweit and D. Rathlev, *$W\gamma$ and $Z\gamma$ production at the LHC in NNLO QCD*, *JHEP* **07** (2015) 085 [arXiv:1504.01330] [INSPIRE].

[71] J.M. Campbell, T. Neumann and C. Williams, *$Z\gamma$ production at NNLO including anomalous couplings*, *JHEP* **11** (2017) 150 [arXiv:1708.02925] [INSPIRE].

[72] T. Gehrmann, N. Glover, A. Huss and J. Whitehead, *Scale and isolation sensitivity of diphoton distributions at the LHC*, *JHEP* **01** (2021) 108 [arXiv:2009.11310] [INSPIRE].

[73] T. Gehrmann et al., *W^+W^- production at hadron colliders in next to next to leading order QCD*, *Phys. Rev. Lett.* **113** (2014) 212001 [arXiv:1408.5243] [INSPIRE].

JHEP01(2022)072

[74] M. Grazzini, S. Kallweit, S. Pozzorini, D. Rathlev and M. Wiesemann, W^+W^- *production at the LHC: fiducial cross sections and distributions in NNLO QCD*, *JHEP* **08** (2016) 140 [arXiv:1605.02716] [INSPIRE].

[75] M. Grazzini, S. Kallweit, D. Rathlev and M. Wiesemann, $W^\pm Z$ *production at hadron colliders in NNLO QCD*, *Phys. Lett. B* **761** (2016) 179 [arXiv:1604.08576] [INSPIRE].

[76] M. Grazzini, S. Kallweit, D. Rathlev and M. Wiesemann, $W^\pm Z$ *production at the LHC: fiducial cross sections and distributions in NNLO QCD*, *JHEP* **05** (2017) 139 [arXiv:1703.09065] [INSPIRE].

[77] D. de Florian and J. Mazzitelli, *Higgs boson pair production at next-to-next-to-leading order in QCD*, *Phys. Rev. Lett.* **111** (2013) 201801 [arXiv:1309.6594] [INSPIRE].

[78] D. de Florian et al., *Differential Higgs boson pair production at next-to-next-to-leading Order in QCD*, *JHEP* **09** (2016) 151 [arXiv:1606.09519] [INSPIRE].

[79] M. Grazzini et al., *Higgs boson pair production at NNLO with top quark mass effects*, *JHEP* **05** (2018) 059 [arXiv:1803.02463] [INSPIRE].

[80] J. Baglio, A. Djouadi, R. Gröber, M.M. Mühlleitner, J. Quevillon and M. Spira, *The measurement of the Higgs self-coupling at the LHC: theoretical status*, *JHEP* **04** (2013) 151 [arXiv:1212.5581] [INSPIRE].

[81] H.T. Li and J. Wang, *Fully differential Higgs pair production in association with a W boson at next-to-next-to-leading order in QCD*, *Phys. Lett. B* **765** (2017) 265 [arXiv:1607.06382] [INSPIRE].

[82] D. de Florian, I. Fabre and J. Mazzitelli, *Triple Higgs production at hadron colliders at NNLO in QCD*, *JHEP* **03** (2020) 155 [arXiv:1912.02760] [INSPIRE].

[83] M. Czakon, R.V. Harlander, J. Klappert and M. Niggetiedt, *Exact top-quark mass dependence in hadronic Higgs production*, *Phys. Rev. Lett.* **127** (2021) 162002 [arXiv:2105.04436] [INSPIRE].

[84] G. Heinrich, *Collider physics at the precision frontier*, *Phys. Rept.* **922** (2021) 1 [arXiv:2009.00516] [INSPIRE].

[85] H.A. Chawdhry, M.L. Czakon, A. Mitov and R. Poncelet, *NNLO QCD corrections to three-photon production at the LHC*, *JHEP* **02** (2020) 057 [arXiv:1911.00479] [INSPIRE].

[86] S. Kallweit, V. Sotnikov and M. Wiesemann, *Triphoton production at hadron colliders in NNLO QCD*, *Phys. Lett. B* **812** (2021) 136013 [arXiv:2010.04681] [INSPIRE].

[87] M. Czakon, A. Mitov and R. Poncelet, *Next-to-next-to-leading order study of three-jet production at the LHC*, *Phys. Rev. Lett.* **127** (2021) 152001 [arXiv:2106.05331] [INSPIRE].

[88] H.A. Chawdhry, M. Czakon, A. Mitov and R. Poncelet, *NNLO QCD corrections to diphoton production with an additional jet at the LHC*, *JHEP* **09** (2021) 093 [arXiv:2105.06940] [INSPIRE].

[89] K. Hamilton, P. Nason, C. Oleari and G. Zanderighi, *Merging* $H/W/Z + 0$ *and* 1 *jet at NLO with no merging scale: a path to parton shower + NNLO matching*, *JHEP* **05** (2013) 082 [arXiv:1212.4504] [INSPIRE].

[90] K. Hamilton, P. Nason, E. Re and G. Zanderighi, *NNLOPS simulation of Higgs boson production*, *JHEP* **10** (2013) 222 [arXiv:1309.0017] [INSPIRE].

[91] A. Karlberg, E. Re and G. Zanderighi, *NNLOPS accurate Drell-Yan production*, *JHEP* **09** (2014) 134 [arXiv:1407.2940] [INSPIRE].

JHEP01(2022)072

[92] W. Astill, W. Bizon, E. Re and G. Zanderighi, *NNLOPS accurate associated HW production*, *JHEP* **06** (2016) 154 [arXiv:1603.01620] [INSPIRE].

[93] W. Astill, W. Bizoń, E. Re and G. Zanderighi, *NNLOPS accurate associated HZ production with $H \to b\bar{b}$ decay at NLO*, *JHEP* **11** (2018) 157 [arXiv:1804.08141] [INSPIRE].

[94] E. Re, M. Wiesemann and G. Zanderighi, *NNLOPS accurate predictions for W^+W^- production*, *JHEP* **12** (2018) 121 [arXiv:1805.09857] [INSPIRE].

[95] S. Höche, Y. Li and S. Prestel, *Higgs-boson production through gluon fusion at NNLO QCD with parton showers*, *Phys. Rev. D* **90** (2014) 054011 [arXiv:1407.3773] [INSPIRE].

[96] S. Höche, Y. Li and S. Prestel, *Drell-Yan lepton pair production at NNLO QCD with parton showers*, *Phys. Rev. D* **91** (2015) 074015 [arXiv:1405.3607] [INSPIRE].

[97] S. Alioli et al., *Combining higher-order resummation with multiple NLO calculations and parton showers in GENEVA*, *JHEP* **09** (2013) 120 [arXiv:1211.7049] [INSPIRE].

[98] S. Alioli, C.W. Bauer, C. Berggren, F.J. Tackmann, J.R. Walsh and S. Zuberi, *Matching fully differential NNLO calculations and parton showers*, *JHEP* **06** (2014) 089 [arXiv:1311.0286] [INSPIRE].

[99] S. Alioli, C.W. Bauer, C. Berggren, F.J. Tackmann and J.R. Walsh, *Drell-Yan production at NNLL'+NNLO matched to parton showers*, *Phys. Rev. D* **92** (2015) 094020 [arXiv:1508.01475] [INSPIRE].

[100] S. Alioli, A. Broggio, S. Kallweit, M.A. Lim and L. Rottoli, *Higgsstrahlung at NNLL'+NNLO matched to parton showers in GENEVA*, *Phys. Rev. D* **100** (2019) 096016 [arXiv:1909.02026] [INSPIRE].

[101] S. Alioli et al., *Precise predictions for photon pair production matched to parton showers in GENEVA*, *JHEP* **04** (2021) 041 [arXiv:2010.10498] [INSPIRE].

[102] S. Alioli et al., *Resummed predictions for hadronic Higgs boson decays*, *JHEP* **04** (2021) 254 [arXiv:2009.13533] [INSPIRE].

[103] S. Alioli et al., *Next-to-next-to-leading order event generation for Z boson pair production matched to parton shower*, *Phys. Lett. B* **818** (2021) 136380 [arXiv:2103.01214] [INSPIRE].

[104] T. Cridge, M.A. Lim and R. Nagar, *$W\gamma$ production at NNLO+PS accuracy in GENEVA*, arXiv:2105.13214 [INSPIRE].

[105] S. Alioli et al., *Matching NNLO predictions to parton showers using N3LL color-singlet transverse momentum resummation in geneva*, *Phys. Rev. D* **104** (2021) 094020 [arXiv:2102.08390] [INSPIRE].

[106] P.F. Monni, P. Nason, E. Re, M. Wiesemann and G. Zanderighi, *MiNNLO$_{PS}$: a new method to match NNLO QCD to parton showers*, *JHEP* **05** (2020) 143 [arXiv:1908.06987] [INSPIRE].

[107] P.F. Monni, E. Re and M. Wiesemann, *MiNNLO$_{PS}$: optimizing $2 \to 1$ hadronic processes*, *Eur. Phys. J. C* **80** (2020) 1075 [arXiv:2006.04133] [INSPIRE].

[108] D. Lombardi, M. Wiesemann and G. Zanderighi, *Advancing MiNNLO$_{\rm PS}$ to diboson processes: $Z\gamma$ production at NNLO+PS*, *JHEP* **06** (2021) [arXiv:2010.10478] [INSPIRE].

[109] D. Lombardi, M. Wiesemann and G. Zanderighi, *W^+W^- production at NNLO+PS with MINNLO$_{PS}$*, *JHEP* **11** (2021) 230 [arXiv:2103.12077] [INSPIRE].

[110] J. Mazzitelli, P.F. Monni, P. Nason, E. Re, M. Wiesemann and G. Zanderighi, *Next-to-next-to-leading order event generation for top-quark pair production*, *Phys. Rev. Lett.* **127** (2021) 062001 [arXiv:2012.14267] [INSPIRE].

JHEP01(2022)072

[111] P. Nason, *A new method for combining NLO QCD with shower Monte Carlo algorithms*, *JHEP* **11** (2004) 040 [hep-ph/0409146] [INSPIRE].

[112] S. Frixione, P. Nason and C. Oleari, *Matching NLO QCD computations with Parton Shower simulations: the POWHEG method*, *JHEP* **11** (2007) 070 [arXiv:0709.2092] [INSPIRE].

[113] S. Alioli, P. Nason, C. Oleari and E. Re, *A general framework for implementing NLO calculations in shower Monte Carlo programs: the POWHEG BOX*, *JHEP* **06** (2010) 043 [arXiv:1002.2581] [INSPIRE].

[114] T. Ježo and P. Nason, *On the treatment of resonances in next-to-leading order calculations matched to a parton shower*, *JHEP* **12** (2015) 065 [arXiv:1509.09071] [INSPIRE].

[115] M. Grazzini, S. Kallweit and M. Wiesemann, *Fully differential NNLO computations with MATRIX*, *Eur. Phys. J. C* **78** (2018) 537 [arXiv:1711.06631] [INSPIRE].

[116] P. Nason and G. Ridolfi, *A positive-weight next-to-leading-order Monte Carlo for Z pair hadroproduction*, *JHEP* **08** (2006) 077 [hep-ph/0606275] [INSPIRE].

[117] F. Cascioli, P. Maierhofer and S. Pozzorini, *Scattering amplitudes with open loops*, *Phys. Rev. Lett.* **108** (2012) 111601 [arXiv:1111.5206] [INSPIRE].

[118] F. Buccioni, S. Pozzorini and M. Zoller, *On-the-fly reduction of open loops*, *Eur. Phys. J. C* **78** (2018) 70 [arXiv:1710.11452] [INSPIRE].

[119] F. Buccioni et al., *OpenLoops 2*, *Eur. Phys. J. C* **79** (2019) 866 [arXiv:1907.13071] [INSPIRE].

[120] T. Gehrmann, A. von Manteuffel and L. Tancredi, *The* VVAMP *project*, available at http://vvamp.hepforge.org.

[121] T. Gehrmann, A. von Manteuffel and L. Tancredi, *The two-loop helicity amplitudes for* $q\bar{q}' \to V_1V_2 \to 4$ *leptons*, *JHEP* **09** (2015) 128 [arXiv:1503.04812] [INSPIRE].

[122] G.P. Salam and J. Rojo, *A Higher Order Perturbative Parton Evolution Toolkit (HOPPET)*, *Comput. Phys. Commun.* **180** (2009) 120 [arXiv:0804.3755] [INSPIRE].

[123] T. Gehrmann and E. Remiddi, *Numerical evaluation of harmonic polylogarithms*, *Comput. Phys. Commun.* **141** (2001) 296 [hep-ph/0107173] [INSPIRE].

[124] P. Nason and C. Oleari, *Generation cuts and Born suppression in POWHEG*, arXiv:1303.3922 [INSPIRE].

[125] T. Ježo, J.M. Lindert, P. Nason, C. Oleari and S. Pozzorini, *An NLO+PS generator for* $t\bar{t}$ *and* Wt *production and decay including non-resonant and interference effects*, *Eur. Phys. J. C* **76** (2016) 691 [arXiv:1607.04538] [INSPIRE].

[126] A. von Manteuffel and L. Tancredi, *The two-loop helicity amplitudes for* $gg \to V_1V_2 \to 4$ *leptons*, *JHEP* **06** (2015) 197 [arXiv:1503.08835] [INSPIRE].

[127] B. Agarwal, S.P. Jones and A. von Manteuffel, *Two-loop helicity amplitudes for* $gg \to ZZ$ *with full top-quark mass effects*, *JHEP* **05** (2021) 256 [arXiv:2011.15113] [INSPIRE].

[128] C. Brønnum-Hansen and C.-Y. Wang, *Top quark contribution to two-loop helicity amplitudes for Z boson pair production in gluon fusion*, *JHEP* **05** (2021) 244 [arXiv:2101.12095] [INSPIRE].

[129] T. Sjöstrand et al., *An introduction to PYTHIA 8.2*, *Comput. Phys. Commun.* **191** (2015) 159 [arXiv:1410.3012] [INSPIRE].

[130] ATLAS collaboration, *ATLAS PYTHIA 8 tunes to 7 TeV data*, ATL-PHYS-PUB-2014-021 (2014).

JHEP01(2022)072

[131] F. Cascioli, S. Höche, F. Krauss, P. Maierhöfer, S. Pozzorini and F. Siegert, *Precise Higgs-background predictions: merging NLO QCD and squared quark-loop corrections to four-lepton + 0, 1 jet production*, *JHEP* **01** (2014) 046 [arXiv:1309.0500] [INSPIRE].

[132] J.M. Campbell, R.K. Ellis, E. Furlan and R. Röntsch, *Interference effects for Higgs boson mediated Z-pair plus jet production*, *Phys. Rev. D* **90** (2014) 093008 [arXiv:1409.1897] [INSPIRE].

[133] C. Li, Y. An, C. Charlot, R. Covarelli, Z. Guan and Q. Li, *Loop-induced ZZ production at the LHC: An improved description by matrix-element matching*, *Phys. Rev. D* **102** (2020) 116003 [arXiv:2006.12860] [INSPIRE].

[134] A. Denner, S. Dittmaier, M. Roth and D. Wackeroth, *Predictions for all processes $e^+e^- \to 4$ fermions + γ*, *Nucl. Phys. B* **560** (1999) 33 [hep-ph/9904472] [INSPIRE].

[135] PARTICLE DATA GROUP collaboration, *Review of particle physics*, *PTEP* **2020** (2020) 083C01 [INSPIRE].

[136] A. Buckley et al., *LHAPDF6: parton density access in the LHC precision era*, *Eur. Phys. J. C* **75** (2015) 132 [arXiv:1412.7420] [INSPIRE].

[137] A. Manohar, P. Nason, G.P. Salam and G. Zanderighi, *How bright is the proton? A precise determination of the photon parton distribution function*, *Phys. Rev. Lett.* **117** (2016) 242002 [arXiv:1607.04266] [INSPIRE].

[138] A.V. Manohar, P. Nason, G.P. Salam and G. Zanderighi, *The photon content of the proton*, *JHEP* **12** (2017) 046 [arXiv:1708.01256] [INSPIRE].

[139] NNPDF collaboration, *Illuminating the photon content of the proton within a global PDF analysis*, *SciPost Phys.* **5** (2018) 008 [arXiv:1712.07053] [INSPIRE].

[140] M. Czakon, D. Heymes and A. Mitov, *Dynamical scales for multi-TeV top-pair production at the LHC*, *JHEP* **04** (2017) 071 [arXiv:1606.03350] [INSPIRE].

[141] F. Caola, F.A. Dreyer, R.W. McDonald and G.P. Salam, *Framing energetic top-quark pair production at the LHC*, *JHEP* **07** (2021) 040 [arXiv:2101.06068] [INSPIRE].

[142] M. Cacciari, G.P. Salam and G. Soyez, *The anti-k_t jet clustering algorithm*, *JHEP* **04** (2008) 063 [arXiv:0802.1189] [INSPIRE].

[143] M. Cacciari, G.P. Salam and G. Soyez, *FastJet user manual*, *Eur. Phys. J. C* **72** (2012) 1896 [arXiv:1111.6097] [INSPIRE].

[144] S. Kallweit, E. Re, L. Rottoli and M. Wiesemann, *Accurate single- and double-differential resummation of colour-singlet processes with MATRIX+RADISH: W^+W^- production at the LHC*, *JHEP* **12** (2020) 147 [arXiv:2004.07720] [INSPIRE].

[145] P.F. Monni, E. Re and P. Torrielli, *Higgs transverse-momentum resummation in direct space*, *Phys. Rev. Lett.* **116** (2016) 242001 [arXiv:1604.02191] [INSPIRE].

[146] W. Bizon, P.F. Monni, E. Re, L. Rottoli and P. Torrielli, *Momentum-space resummation for transverse observables and the Higgs $p_\perp$ at N^3LL+NNLO*, *JHEP* **02** (2018) 108 [arXiv:1705.09127] [INSPIRE].

[147] S. Bräuer, A. Denner, M. Pellen, M. Schönherr and S. Schumann, *Fixed-order and merged parton-shower predictions for WW and WWj production at the LHC including NLO QCD and EW corrections*, *JHEP* **10** (2020) 159 [arXiv:2005.12128] [INSPIRE].

JHEP01(2022)072